

Article

## A Global Grassland Drought Index (GDI) Product: Algorithm and Validation

Binbin He \*, Zhanmang Liao, Xingwen Quan, Xing Li and Junjie Hu

School of Resources and Environment, University of Electronic Science and Technology of China, No. 2006, Xiyuan Avenue, West Hi-Tech Zone, Chengdu 611731, China;

E-Mails: dajuzidesky@163.com (Z.L.); quanxw7@gmail.com (X.Q.); zxwlxty@163.com (X.L.); junjiehu2013@163.com (J.H.)

\* Author to whom correspondence should be addressed; E-Mail: binbinhe@uestc.edu.cn.

Academic Editors: Xin Li, Yuei-An Liou, Qinhua Liu, Ioannis Gitas and Prasad S. Thenkabail

Received: 21 July 2015 / Accepted: 22 September 2015 / Published: 28 September 2015

---

**Abstract:** Existing drought indices have been widely used to monitor meteorological drought and agricultural drought; however, few of them are focus on drought monitoring for grassland regions. This study presented a new drought index, the Grassland Drought Index (GDI), for monitoring drought conditions in global grassland regions. These regions are vital for the environment and human society but susceptible to drought. The GDI was constructed based on three measures of water content: precipitation, soil moisture (SM), and canopy water content (CWC). The precipitation information was extracted from the available precipitation datasets, and SM was estimated by downscaling exiting soil moisture data to a 1 km resolution, and CWC was retrieved based on the PROSAIL (PROSPECT + SAIL) model. Each variable was scaled from 0 to 1 for each pixel based on absolute minimum and maximum values over time, and these scaled variables were combined with the selected weights to construct the GDI. According to validation at the regional scale, the GDI was correlated with the Standardized Precipitation Index (SPI) to some extent, and captured most of the drought area identified by the United States Drought Monitor (USDM) maps. In addition, the global GDI product at a 1 km spatial resolution substantially agreed with the global Standardized Precipitation Evapotranspiration Index (SPEI) product throughout the period 2005–2010, and it provided detailed and accurate information about the location and the duration of drought based on the evaluation using the known drought events.

**Keywords:** drought monitoring; grassland; grassland drought index (GDI); precipitation; soil moisture content; canopy water content; global GDI product; global SPEI product

---

## 1. Introduction

Drought is a major environmental disaster, and affects numerous people and various trades [1]. Drought monitoring and forecasting techniques are crucial for reducing society's vulnerability to drought and its subsequent impacts and will lead to better drought-management practices [2]. Grasslands are among the world's most widely distributed vegetation types. The importance of the grasslands lies not only in their vast coverage but also in the diverse benefits they produce [3]. They provide valuable ecological services, such as nutrient cycling and the storage of carbon, and improve local economies by supporting the livestock industry and recreational activities such as tourist. However, because grasslands are generally located in arid and semi-arid regions, they are highly susceptible to drought. Developing an effective drought monitoring method for grasslands is imperative.

Based on the meteorological observations, in recent decades, a series of classical climatic drought indices have been successfully developed to evaluate drought. However, the network of meteorological stations often lacks continuous spatial coverage, especially in mountainous regions [4]. Thus, spatial interpolation is a common method to obtain a continuous spatial distribution of drought conditions based on data from meteorological stations, but there may be considerable uncertainties involved in such an approach because many factors affect the interpolation process [5].

The remote sensing community defines drought as a period of abnormally dry weather that changes the vegetation cover [6,7]. Therefore, drought severity can be estimated by monitoring vegetation conditions. Additionally, as it entails pressures from deficient precipitation, drought causes other climate anomalies such as high temperature and low soil moisture and relative humidity [8]. These phenomena allow new approaches to monitor drought and encourage the development of remote sensing based drought monitoring. Using satellite remote sensing to monitor drought offers numerous advantages compared with traditional drought monitoring [9]: (1) The high spatial resolution of remote sensing data; (2) the large coverage of satellite sensors, which reduces the difficulty associated with large-scale drought monitoring; (3) the availability of data for regions with a low density of weather stations; and (4) the ability to conduct drought monitoring from various perspectives by utilizing multi-spectral and multi-angle information on surface features. A review about current and emerging drought monitoring approaches using satellite remote sensing observations can be obtained in [10].

To date, numerous studies have been conducted related to drought monitoring and the influence of drought on the ecosystem, and there are systems that provide global drought information, such as the University of Washington's Surface Water Monitor [11,12], Global Integrated Drought Monitoring and Prediction System [13], and US-Mexico Drought Prediction Tool [14]. The existing drought indices can be roughly divided into five categories [6,15].

The first category includes classical climatic drought indices based on meteorology measurements. One of the most widely used indices was developed by Palmer in 1965. To better monitor drought in terms of its intensity, duration, and spatial extent, Palmer's original index was extended to create the

Palmer Drought Severity Index (PDSI) [16–18]. However, the inherent timescale of 9–12 months makes the PDSI unsuited for assessing long-term hydrological drought impacts. In contrast, based on precipitation data, the Standardized Precipitation Index (SPI) proposed by McKee [19] allows for calculation at multiple timescales to identify the influence of droughts at different timescales [17,19,20]. The 1-month SPI reflects short-term drought conditions and relates to the moisture of the superficial soil. The 6- and 9-month SPI measures depict the medium-term trend in precipitation patterns, and are related to soil moisture in deeper layers. The Standardized Precipitation Evapotranspiration Index (SPEI) was constructed based on a combination of the PDSI's sensitivity to changes in evaporative demand (caused by temperature fluctuations and trends) and the SPI's simplicity of calculation and multi-temporal nature. The SPEI is particularly well suited to detect the effects of global warming on drought conditions [21].

The second category of drought indices monitor drought by evaluating vegetation conditions. One class of these indices are vegetation greenness indices, and the representative indices in this class are the Normalized Difference Vegetation Index (NDVI) [22] and the Enhanced Vegetation Index (EVI) [23], which indicate the growth vigor of the vegetation. Another class includes the vegetation water indices based on the water content of the vegetation, such as the Normalized Difference Infrared Index (NDII) [24] and the Water Band Index (WBI) [25]. These indices play the important role of accurately monitoring the influence of a drought on vegetation, but they cannot distinguish drought-related vegetation stress from other factors that cause vegetation changes. Moreover, real-time drought monitoring is difficult to achieve because of the time delay with which vegetation reacts to drought [26–28].

The third category of drought indices monitor drought using thermal emission patterns. Land Surface Temperature (LST), which is directly related to the net radiation flux and surface moisture conditions, represents the instantaneous state of energy flux for a land surface. By using thermal emission patterns in combination with meteorological observations, drought can be detected before vegetation degradation occurs [29]. The representative index in this case is the Temperature Condition Index (TCI), which is constructed by normalizing the LST via its historical maximum and minimum values. Generally, these types of drought indices are combined with other information to improve monitoring accuracy [30,31], for example, by improving the ability to differentiate between the drought-caused vegetation stress and other factors in vegetation drought monitoring.

The fourth category of drought indices monitor drought exploiting information on hydrologic soil properties. A lack of precipitation will directly affect soil moisture content in certain regions, and thus, drought can be monitored by estimating soil moisture content. The Soil Moisture Deficit Index (SMDI), which monitors drought by calculating the weekly soil moisture deficit, is the representative index of this category [32]. The Temperature Vegetation Dryness Index (TVDI), based on the relationship between NDVI and temperature, is highly correlated with soil moisture, and it also belongs to the category of moisture index methods for monitoring drought [33,34].

Finally, indices in the fifth category are developed by integrating multiple measurements. Because drought is a complex phenomenon, it is difficult to derive an accurate estimation of drought conditions using a single type of information or one-sided studies. Therefore, the integrated indices that combine multiple types of data offer advantages and have been widely developed. The Vegetation Health Index (VHI) was proposed and is based on the combining the scaled NDVI and LST. It was found to be very useful for early drought detection and monitoring the impacts of droughts on crop and pasture production [35–37]. Rhee proposed the Scaled Drought Condition Index (SDCI) for agricultural drought

monitoring in both arid and humid regions by integrating the data of precipitation, NDVI and LST [5]. Abbas used the Vegetation Supply Water Index (NVSWI), calculated as the ratio of the NDVI to the LST, to characterize the development of drought conditions in central Yunnan Province, China [38]. Combining remote sensing data with *in situ* data from a relatively dense network, such as the Vegetation Drought Response Index (VegDRI) has proven extremely useful [5,28]. By including six key physical indicators and many supplementary indicators, United States Drought Monitor (USDM) maps have been published online as weekly product for drought monitoring in the US [2].

Although a variety of drought indices have been proposed to monitor drought and offer different advantages according to the summary above, it is difficult to establish an index that is suitable for all regions and land cover types because droughts can produce different types of changes simultaneously, and these changes may be interpreted in different ways [8].

We concentrated on drought monitoring for grassland. It is highly beneficial for the regional and global environment. Based on the available information on the water cycle in grassland regions, we selected three layers (air, soil and plants) of the grassland ecosystem as the key factors for monitoring drought. Three indicators for the three layers—precipitation, soil moisture (SM), and canopy water content (CWC)—were calculated using multiple-sensor data and then combined to construct a new drought index, which we named Grassland Drought Index (GDI), to monitor degree of drought for grassland areas. Additionally, we verified the retrieval accuracy of the CWC data using Landsat 8 images and *in situ* measured data. We then quantitatively and qualitatively validated the drought-monitoring performance of the GDI using the SPI and USDM map, respectively. Our global GDI product for global grassland regions was calculated on a monthly basis over the period 2005–2010, and we then employed the global SPEI product to evaluate the ability of the GDI to capture drought in grassland regions across the globe.

## 2. Data

Three types of data—data from meteorological stations, remote sensing data, and ancillary data—were used in this study. The meteorological station data and ancillary data were obtained for the validation process, and the calculation of the GDI was solely based on remote sensing data. Moreover, two sets of remote sensing data were used to validate the GDI at the regional scale and the global GDI product which are both at a spatial resolution of 1 km. For the GDI at the regional scale, the CWC at a 1 km spatial resolution was calculated using the Leaf Area Index (LAI) data and reflectance data from the Moderate Resolution Imaging Spectroradiometer (MODIS), SM was estimated by downscaling the Advanced Microwave Scanning Radiometer (AMSR-E) soil moisture data from 25 km to 1 km, and the precipitation data were directly extracted from the 25-km Tropical Rainfall Measuring Mission (TRMM) monthly precipitation data. To produce the global GDI product, we replaced the AMSR-E soil moisture and the TRMM monthly data with the Global Land Data Assimilation System (GLDAS) soil moisture data at a spatial resolution of 25 km and the Climate Research Unit (CRU) monthly precipitation data at a spatial resolution of 55 km, respectively, to improve the output of the global product. The details of the data we employed are presented below.

## 2.1. Meteorological Station Data

The SPI, developed by McKee [19], is one of the most widely used drought indices. To calculate SPI, the frequency distribution of precipitation should be constructed using the precipitation data. Then, a gamma probability density function is fitted to the frequency distribution of precipitation, and transformed into the standard normal distribution to obtain the SPI value. By cumulating different timescales of precipitation to construct the frequency distribution, it is possible to obtain the SPI for multiple timescales. A negative value of the SPI means that the region is facing a drought, and the more severe a drought is, the lower the SPI value will be [19,39,40].

To obtain a SPI to validate the performance of the GDI, we obtained monthly precipitation records from all weather stations throughout China for the period 1971–2010 from the China Meteorological Data Sharing Service System [41]. A total of 194 stations located in all types of land cover were available, but only weather stations located in grassland areas were included in the analysis. Based on the land cover product MCD12Q1, data from 49 stations located in grassland regions for more than six years during the period 2002–2010 were extracted.

## 2.2. Remote Sensing Data

### 2.2.1. MODIS Data

Four types of MODIS products were used to conduct our experiments. For the validation experiment at the regional scale, we selected data for 13 August during the period 2002–2010 to monitor the extent of drought in the region. To produce the global GDI product, the data from a time interval of 32 days and beginning on 1 January in each year during the period 2005–2010 were chosen to produce the monthly GDI product. The details of our chosen MODIS products are as follows: (1) Land cover classifications used to locate the grassland regions were derived from MODIS data (MCD12Q1) with a spatial resolution of 500 m. This approach identifies 17 land cover types as defined by the International Geosphere-Biosphere Program (IGBP). (2) Global surface reflectance values were derived from MYD09A1 with a spatial resolution of 500 m, and the bands used to calculate the NDVI and NDII include red, near infrared and short infrared. (3) An important vegetation structural parameter, the LAI was obtained from MOD15A2 at a spatial resolution of 1 km. (4) The LST at a spatial resolution of 1 km was extracted from MOD11A2, and the daytime LST was used. All MODIS data were obtained from the Level 1 and Atmosphere Archive and Distribution System (LAADS) [42]. Moreover, the MODIS data that are not at a 1 km resolution were resampled at 1 km to address the difference in spatial resolution.

### 2.2.2. AMSR-E and GLDAS Soil Moisture

To validate the GDI at the regional scale, the soil moisture data used in the study were derived from the AMSR-E Level-3 land surface product (AE\_Land3) of the Earth Observing System (EOS) which was developed by the National Space Development Agency of Japan (NASDA) and provided to the US National Aeronautics and Space Administration (NASA). The data were obtained from the National Snow and Ice Data Center (NSIDC) [43] and are at an approximate spatial resolution of 25 km [44,45]. Because AMSR-E soil moisture data are provided on a daily basis and most MODIS data considered in

this study are 8-day tiled products, we calculated the average soil moisture using the ascending and descending bands of the AMSR-E data from the 8 days of MODIS data to conform to the timescale of the MODIS data.

Because AMSR-E soil moisture information is daily data, it would be time-consuming to produce a long-term GDI product, moreover, its temporal coverage is only in 2002–2011. We replaced the AMSR-E data with the GLDAS Noah Land Surface Model L4 monthly  $0.25 \times 0.25$  degree Version 2.0, which provides convenient access to the long-term data. These data are generated on a monthly basis by temporally averaging 3-hourly data, contain a series of land surface parameters simulated from the Noah Model 3.3, and currently cover the period 1948–2010 [46,47]. The data from January 2005 to December 2010 were acquired to produce the monthly global GDI product from the Goddard Earth Sciences Data and Information Services Center (GES DISC) [48].

### 2.2.3. TRMM and CRU Precipitation

The TRMM, successfully launched in 1997 from the Tanegashima Space Center in Japan, is a joint U.S.-Japan satellite mission to monitor tropical and subtropical precipitation and to estimate the associated latent heating. Its monthly rainfall data, the 3B43 dataset were used as the remote sensing precipitation data. Estimated from 3-hourly multi-satellite fields, it primarily covers tropical regions with a latitude band that ranges from  $50^\circ$  south to  $50^\circ$  north, has a spatial resolution of  $0.25^\circ$  and produces data in the form of a monthly precipitation rate (mm/h). The 2002–2010 datasets were obtained from the GES DISC [48]. Given their relatively high spatial resolution compared with CRU data and the non-global coverage of the TRMM data, TRMM data were used to validate the GDI at a regional scale.

The University of East Anglia developed the CRU dataset. Because of their global coverage, we chose CRU monthly precipitation data as the input to produce the global GDI product. The CRU TS (time-series) 3.21 datasets were chosen in the study, which provide the variations in climate over the period 1901–2012 and are on resolution grids of  $0.5 \times 0.5$  degrees. The datasets from 2005–2010 were obtained at [49].

### 2.2.4. SPEI Data

Based on a water balance framework, the SPEI is calculated using both precipitation and temperature data, and it has the advantage of realizing the combination of the multiscalar character and effects of temperature variability on drought assessment [21]. The global SPEI was selected because of its advantages and the convenience of obtaining its data to verify the performance of the GDI for global grassland regions. The global SPEI values from January 2005 to December 2010 were obtained from the SPEI Global Drought Monitor [50], which offers nearly real-time information on drought conditions on a global scale with the time-scales between 1 and 48 months [51]. Based on the Thornthwaite Equation [52], the SPEI data at a  $0.5$  degree spatial resolution and a time scale of six months were used in the study.

## 2.3. Ancillary Data

### 2.3.1. Ground-Measured Data

The ground-measured data were used to verify the accuracy of CWC retrieval. The field survey was conducted from 2–7 August 2013 in Ruogai Prairie, Sichuan Province, China. A total of fifty sampling

plots (30 m × 30 m) were chosen in flat and homogenous grassland regions which were at least 300 m away from the roads, and were located using the Global Positioning System (GPS). The aboveground grass was clipped from three randomly selected plots (0.5 m × 0.5 m) within each sampling site and were then immediately sealed and transported to the laboratory. When obtaining *in situ* CWC of the grass, only the leaves of the fresh grass were weighed (fresh weight) while the stems and roots were removed. Dried for 48 hours at 70 °C, the grass was weighed again (dry weight). The CWC was obtained as the difference in values between the fresh weight and the dry weight of the sampled grass.

### 2.3.2. USDM Maps

The USDM, which provides weekly information on drought conditions in US, was selected to validate our proposed GDI. Established in 1999, it is produced jointly by the National Oceanic and Atmospheric Administration, the U.S. Department of Agriculture and the National Drought Mitigation Center (NDMC) at the University of Nebraska-Lincoln. Its severity categories are based on six key physical indicators and numerous supplementary indicators. The six indicators include the PDSI, Climate Prediction Center (CPC) Soil Moisture Model Percentiles, U.S. Geological Survey (USGS) Daily Streamflow Percentiles, the SPI, and remotely sensed satellite VHI. Ancillary indicators include the Palmer Crop Moisture Index (CMI), the Keetch-Bryam Drought Index (KBDI) [2]. The USDM maps for the contiguous US at the end of August over the period 2002–2010 were acquired from the US Drought Monitor [53].

## 3. Methodology

### 3.1. The Basic Theory for Constructing the GDI

Since drought is primarily caused by a lack of water, it is important to understand the water cycle of the grassland ecosystem before constructing the GDI. The simplified water cycle is as follows. The water vapor in the air will condense into water under appropriate conditions and then reach the land surface as rainfall. Some of the precipitation will be directly intercepted by the stems and leaves of plants, and this water will rapidly evaporate into the air. Other water will permeate into the soil and increase the soil's moisture content. If there is enough rainfall, the water in the soil will reach the groundwater layer due to gravitational effects. When the water yield is larger than the soil penetrability or the soil is under a water saturated condition, the surface water will develop into puddle and even runoff. The root systems of plants are generally located in the water unsaturated zone between the ground surface and the groundwater layer, and hence plants generally obtain their water from the unsaturated soil layer. This water will return to the air through transpiration by plants and the evaporation of water contained in the soil [54]. Regarding the trees scattered in grassland which have a developed root system that go deep in the water table, their dependence to rainfall and superficial soil moisture will be reduced.

The summary above offers a brief description of the water cycle on land. If there is a long period of deficient precipitation, the soil moisture content will decline sharply due to transpiration by plants and the evaporation of water in the soil, especially in the water unsaturated layer. This will make it difficult for plant roots to obtain water because the water is tightly bound to the soil particles. As the water content of the grass decreases, the plant will suffer from water deficiency and, in turn, sickness or even death. A

drought will occur unless the region receives rainfall again [8]. However, if the plants are irrigated by farmers or close to rivers, and the soil moisture is sufficient for plants to obtain water for their biological operation, the region will suffer little drought even if precipitation levels are deficient. Consequently, the crucial factor determining whether a drought will occur in a grassland ecosystem is the water content in three layers: the air, the soil, and the vegetation. Single-aspect-based monitoring will not cover the entire relevant scope of drought. Therefore, the new index GDI should comprehensively monitor drought based on these three factors. We chose the three indicators of precipitation, SM and CWC to estimate the water conditions of the air, soil and vegetation, respectively. Then, we combined and weighted them to construct the GDI. Having selected the indicators, another key consideration is the algorithms used to estimate the three indicators.

### 3.2. Retrieving CWC Information

For grassland that is distributed homogeneously along the horizontal dimension, the PROSAIL model, which assumes that the canopy is horizontally homogeneous, is suitable to retrieve the canopy parameters of a grassland ecosystem. Numerous studies employed the PROSAIL models to retrieve the vegetation parameters, such as LAI, CWC, and Live Fuel Moisture Content (LFMC), in grassland regions [55,56]. The PROSAIL model is a combination of the SAILH model and the PROSPECT model to simulate canopy spectral and directional reflectance in the forward and inverse directions [57–59]. Thus, the physiological processes of the plant canopy can be directly related to remote sensing data [60]. The SAIL model is one of the earliest canopy reflectance models to simulate the bidirectional reflectance factor of turbid medium plant canopies, and was adapted by Kuusk in the early 1990s to the SAILH model to take account for the hot spot effect. The PROSPECT model, which was developed at the leaf level, can simulate the spectral reflectance at a scale of 400–2500 nm. It is based on the representation of the leaf as one or several absorbing plates and requires the leaf mesophyll structural parameter  $N$  and the biochemical components of the leaf.

The version of the PROSAIL model used in the study was PROSAIL\_5B [61], which requires the parameterization of 14 parameters. Six input parameters are needed for PROSPECT model: leaf structure parameter,  $N$  (unit-less); leaf chlorophyll content,  $C_{ab}$  ( $\mu\text{g}/\text{cm}^2$ ); equivalent water thickness,  $C_w$  ( $\text{g}/\text{cm}^2$ ); dry matter content,  $C_m$  ( $\text{g}/\text{cm}^2$ ); carotenoid content,  $C_{ar}$  ( $\mu\text{g}/\text{cm}^2$ ) and leaf brown pigment,  $C_{bp}$  (unit-less). Moreover, eight input parameters are needed for SAILH model: the sun zenith angle,  $tts$  ( $^\circ$ ); observer zenith angle,  $tto$  ( $^\circ$ ); relative azimuth angle,  $\psi$  ( $^\circ$ ); soil factor,  $p_{soil}$  (unit-less); LAI ( $\text{m}^2 \times \text{m}^2$ ); hot spot size parameter,  $hspot$  (unit-less) and the two leaf inclination distribution function (LIDF) parameters, LIDFa and LIDFb (unit-less). Performing a sensitivity analysis of the PROSAIL model is useful for reducing the number of input parameters. Because the NDII is sensitive to CWC and is often used to retrieve CWC [62,63], we implemented those parameters that are sensitive to NDII as free variables while the insensitive parameters were specified using fixed empirical values. Following studies by [64], the final free variables we selected are LAI and  $C_w$ .  $C_w$  was set from 0.005 to 0.08; and LAI ranged from 0.1 to 8. Because other parameters are not sensitive to NDII, they were simply determined by empirical values:  $C_m$  was set as 0.009; Leaf mesophyll structure  $N$  was set as 1.5; and LIDF type was empirically set as spherical, where LIDFa =  $-0.35$  and LIDFb =  $-0.15$  (model default values). The rest of the model parameters was set to exponential and model default values because they have no or only slight effects



on NDII. Having parameterized all of the inputs of the PROSAIL model, a look-up table was built to construct the relationship between canopy reflectance and the vegetation parameters. To simplify the retrieval of CWC, we then developed a multiple regression model between NDII and the LAI and Equivalent Water Thickness (EWT) variables based on the look-up table. The CWC can be simply retrieved using a regression model that uses LAI and NDII as inputs. For the rapid change in NDII when LAI falls below 2, we employed two regression equations, one for when LAI is smaller than 2 and one for when it is greater than 2, to obtain a better fitting result. With a coefficient of determination ( $R^2$ ) of 0.9903 and a root-mean-square error (RMSE) of 0.0251, the regression equations we employed are as follows.

When  $LAI \leq 2$ :

$$NDII = -0.8685 + 0.1465 * \log(EWT + 0.0096) + 1.0495 * \log(LAI + 3.1367) \quad (1)$$

When  $LAI > 2$ :

$$NDII = 1.2945 + 0.2442 * \log(EWT + 0.0049) + 0.0679 * \log(LAI - 1.8725) \quad (2)$$

Based on the regression model, the EWT can be retrieved via the inputs of NDII and LAI. Then, the CWC with the unit of  $g/cm^2$  was calculated using  $CWC = EWT \times LAI \times 10000$ . Although the fixed values of the PROSAIL inputs will cause errors in different regions, we ignored such errors for two reasons. First, there is only a single vegetation type in our study and the fixed inputs are not sensitive to the CWC. Second, the CWC will be scaled to relative values using historical values in the next process, and thus the error caused by the fixed inputs will be reduced to some extent. The scaling details are described in Section 3.4. Therefore, we used this regression model to estimate the CWC over the global grassland regions.

### 3.3. The Estimation of SM

The spatial resolution of the global soil moisture datasets is at 25 km which is quite coarse relative to the MODIS data. To calculate the GDI at 1 km, we downscaled the AMSR-E soil moisture data from 25 km to 1 km. According to the studies of Carlson, there is a relationship among soil moisture, NDVI, and LST, which can be expressed through a regression formula [65]. It is possible to downscale AMSR-E soil moisture from 25 to 1 km based on this relationship [66–68].

$$LST^* = \frac{LST - LST_0}{LST_s - LST_0} \quad (3)$$

$$NDVI^* = \frac{NDVI - NDVI_0}{NDVI_s - NDVI_0} \quad (4)$$

$$SM = \sum_{i=0}^{i=n} \sum_{j=0}^{j=n} a_{ij} NDVI^{*(i)} LST^{*(j)} \quad (5)$$

Where subscripts  $o$  and  $s$  denote the minimum and maximum values. SM represents the soil moisture content. Ignoring the third-order and higher-order terms of Equation (5), we can expand it to obtain a second order polynomial as shown in Equation (6), which was used as the regression model to downscale the AMSR-E soil moisture data in our study.

$$SM = a_0 + a_1 NDVI^* + a_2 LST^* + a_3 NDVI^* LST^* + a_4 NDVI^{*2} + a_5 LST^{*2} \quad (6)$$

We removed the cloudy regions from the remote sensing images using the haze optimized transformation (HOT) method proposed by Zhang *et al.* [69], and we also removed regions with invalid values. Based on the clear and reliable data for the selected regions, the 1-km NDVI was calculated using surface reflectance, and the 1-km LST was directly extracted from the MODIS LST product. We then aggregated the NDVI and LST to a 25 km resolution and used these data to determine the regression coefficients for the regression model. Once the regression model was established, the 1 km soil moisture data were estimated by introducing the 1km level NDVI and LST variables into the regression model.

### 3.4. The Normalization and Integration of Precipitation, SM and CWC to Construct GDI

We did not downscale the precipitation data using a scheme similar to that employed to downscale soil moisture; instead, we directly extracted the precipitation data by resampling the TRMM or CRU data at the 1 km level. After the precipitation, SM and CWC variables were acquired, they were all scaled from 0 to 1 for each pixel as Kogan did to construct the VCI using NDVI [30].

$$P_{scaled} = \frac{P - P_{min}}{P_{max} - P_{min}} \quad (7)$$

Where P represents the parameters of precipitation, SM, or CWC. The subscript *scaled* means that the parameters were scaled on the range 0–1, and the subscripts *max* and *min* denote the historical maximum and minimum values for each pixel over time, respectively. Therefore, it is necessary to obtain data for the same day from different years to acquire the historical maximum and minimum values. After normalization, the scaled values can represent the temporal change in the parameters over the years.

As shown in Equation (8), GDI is the combination of the scaled precipitation, SM, and CWC values with selected weights. It is a dimensionless index and ranges 0–1. Moreover, a more severe drought will generate a smaller GDI value.

$$GDI = \omega_1 \times PRE_{scaled} + \omega_2 \times SM_{scaled} + (1 - \omega_1 - \omega_2) \times CWC_{scaled} \quad (8)$$

Where PRE represents the precipitation in the region.  $\omega_1$ ,  $\omega_2$  and  $1 - \omega_1 - \omega_2$  are the weights of the scaled precipitation, soil moisture, and CWC, respectively.

We adopted the three sets of weights used in the work of Rhee and conducted experiments to identify the weights that have the best performance and selected them as the final weights [5,70]. Table 1 shows the details of the weights distribution, and GDI-1, GDI-2, and GDI-3 represents the GDI calculated by different weights. Moreover, to give a clear understand about the used data and the algorithm of GDI, the flowchart of calculating GDI was shown in Figure 1.

**Table 1.** The different GDIs combined with different weights for the scaled precipitation, SM and CWC values.

Drought Indices	Formula
GDI-1	$2/5 \times PRE_{scaled} + 2/5 \times SM_{scaled} + 1/5 \times CWC_{scaled}$
GDI-2	$1/2 \times PRE_{scaled} + 1/4 \times SM_{scaled} + 1/4 \times CWC_{scaled}$
GDI-3	$1/3 \times PRE_{scaled} + 1/3 \times SM_{scaled} + 1/3 \times CWC_{scaled}$

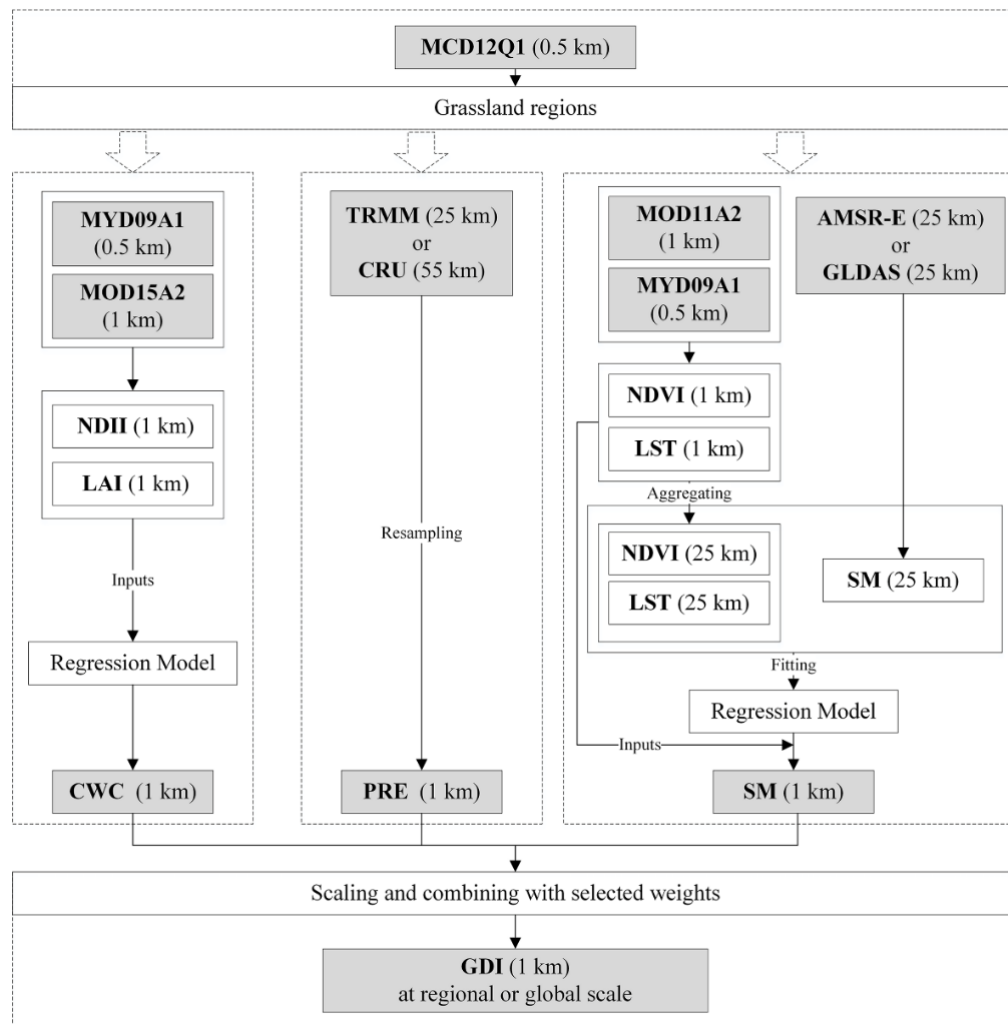


**Figure 1.** Flowchart of calculating GDI. The shown spatial resolution of TRMM, CRU, AMSR-E, and GLDAS are approximate values.

### 3.5. Validation Schemes at the Regional Scale

To assess the performance of the GDI, we conducted three validation schemes at the regional scale for three different validation areas. We first validated the accuracy of the retrieved CWC data, which is one of the components of the GDI, for Ruoergai Prairie, Sichuan Province, China. In the grassland regions of China, we qualitatively validated the GDI by analyzing the correlation between GDI and SPI and then determined the final weights to construct GDI. Based on the USDM maps, which combines multiple information and ground auxiliary data, we conducted a quantitative validation by comparing the spatial distributions reported by the GDI and USDM over the contiguous US.

#### 3.5.1. Validation of the CWC Retrieval Method in Ruoergai Prairie

The validity of the CWC retrieval method in the study was assessed using ground-measured data collected in August 2013. Because the spatial resolution of the MODIS was too coarse compared with the field data, which can only represent conditions in a very limited region, we employed the 30 m Landsat-8 OLI image to conduct the validation process. An image that covers all of the ground sampling

plots in Ruoergai Prairie, Sichuan Province, China, was obtained on 24 July 2013 from the Earth Resources Observation and Science Center (EROS) [71]. The existing MODIS LAI product is at a 1 km spatial resolution, and hence to acquire the LAI at a 30 m resolution, downscaling is necessary. Based on the MODIS EVI and LAI products at a 1 km spatial resolution, we developed a simple regression model between EVI and LAI and then included EVI calculated based on the reflectance data from Landsat in the regression model to obtain the 30 m LAI [55]. NDII was calculated by the red and SWIR Landsat bands. After we obtained NDII and LAI at a 30 m resolution, Equations (1) and (2) were used to acquire the inverse CWC at a spatial resolution of 30 m.

The validation area in this section is located in Ruoergai Prairie, Sichuan Province, China. Most of the area is characterized by grassland, and the remaining areas consist of forests, marshes and shrublands. The climate of the areas is cold with an average annual temperature of 0.7°C and an average annual precipitation of approximately 656.8 mm. It has an average altitude of 3500 m and little relief over grassland regions. The detailed location of Ruoergai is shown in Figure 2.

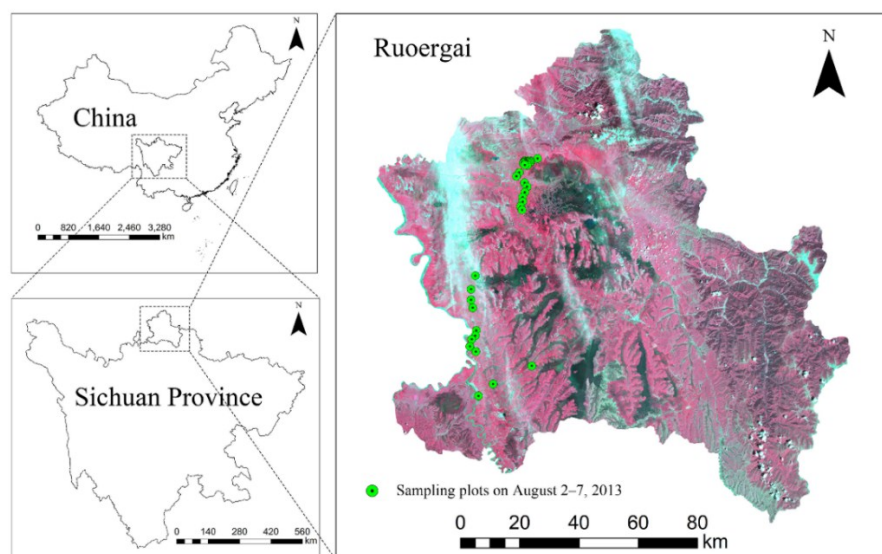


**Figure 2.** Study area for the validation of CWC and the locations of the sampling plots. The map on the right is a composite image from Landsat 8.

### 3.5.2. Quantitatively Validating GDI using *in Situ* SPI for the Grassland Regions of China

SPI has been accepted broadly for research and operational use because of its well-known advantages [20]. It is spatially invariant in the interpretation, and can monitor both short-term water supplies and longer-term water resources such as groundwater supplies. By analyzing the correlation between the GDI and SPI, we can roughly assess the effectiveness of GDI. Having adopted the three sets of weights shown in Table 1, we determined the final weights of air, plants and soil by identifying the weights with the maximum correlation coefficient among them [5,70].

Based on data from meteorological stations data in China, the country's grassland regions were chosen as the validation areas for the quantitative validation of GDI, and these regions cover approximately 4 million km<sup>2</sup>, and the *in situ* SPI was calculated using data from these meteorological stations. According to the classification scheme of IGBP, we considered savanna and woody savanna

areas when dividing the study areas because these two land types are also characterized by herbaceous plants. For simplicity, the “grassland” in the study represents a combination of typical “grassland”, “savanna” and “woody savanna”. The study time was 13 August over the period 2002–2010. Figure 3 shows the detailed distribution of the 49 stations and grassland in China.

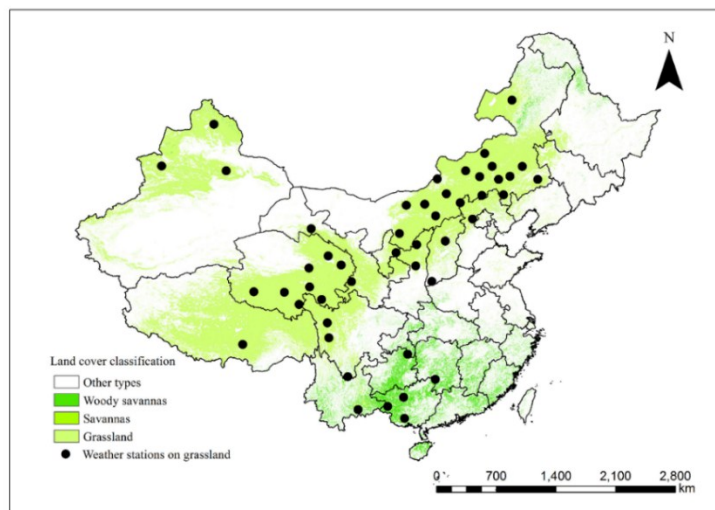


**Figure 3.** The land cover and the position of weather stations in grassland regions in China.

### 3.5.3. Qualitatively Validating GDI Using USDM Maps in the Contiguous US

Drought is a complex natural disaster, and an SPI solely based on precipitation data will be of limited effectiveness when monitoring land surface conditions. USDM maps based on *in situ* measurements, remote sensing data, and expert adjustment will help us to interpret complex drought impacts [2]. USDM is considered to be the current state-of-the art drought monitoring tool for the United States. It is important for GDI to provide comprehensive information as USDM maps do. Therefore, we chose USDM maps to conduct our second validation scheme in this section. Because the USDM maps provide a coarse distribution of the drought category, an exact comparison of drought condition is not appropriate. After color rendering the GDI, we compared the USDM maps and the GDI maps, primarily visually.

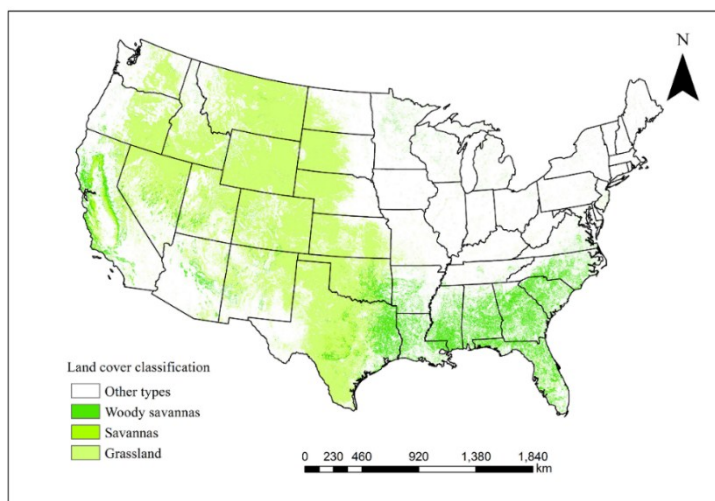


**Figure 4.** The grassland distribution for the contiguous US.

The USDM only monitors drought conditions in the US, and we chose the contiguous US to represent the validation areas in this section. Historically, grasslands occupied approximately one billion acres in US—approximately one half of the landmass of the 48 contiguous states. The majority of the grasslands are located west of the Mississippi River. However, some native grasslands were scattered throughout the Midwestern and Southeastern States [3]. The grassland distribution is shown in Figure 4, constructed based on the MODIS IGBP land cover classification map of 2010 MCD12Q1. According to the classification map, a large proportion of the contiguous US is characterized by grassland, which is primarily located in the western contiguous US.

### 3.6. Producing Schemes of the Global GDI Product

Based on the global data obtained during the period 2005–2010, using a time interval of 32 days and beginning on 1 January, we produced a monthly global GDI at a spatial resolution of 1 km. Due to the large amount of data involved and the resulting heavy computational burden entailed by a global analysis, the Hadoop platform was adopted to improve computational efficiency. The global data were segmented into numerous tile images according to the MODIS Sinusoidal Grid and were then processed using different computing nodes. To calculate SM at a resolution of 1 km, a regression model was developed for every tile image, and the same approach was used to calculate CWC and precipitation. Because the scaled CWC, SM, and precipitation data were acquired for each tile, we obtained the GDI at each tile and then mosaicked them to produce the global distribution of GDI.

## 4. Results and Discussion

### 4.1. Validation Results of the CWC Retrieval Method

Based on the sampling plots at the cloudless regions on the Landsat 8 image, we fitted the relationship between the retrieved CWC and the ground-measured CWC values. Figure 5 shows the scatterplots of the results. The slope of the trend line is 0.62. Though the slope of the trend line is not close to 1, this causes little influence to the GDI because the CWC will be scaled to relative values. The important fitting parameters to evaluate the validity of the CWC is the  $R^2$  and RMSE. The  $R^2$  is 0.62, which shows that the retrieved CWC has a good correlation with the measured CWC, and RMSE is 202.7 g/m<sup>2</sup>. The results verified that the adopted method of CWC retrieval is reliable and achieves the aim of estimating the water condition of the vegetation layer in grassland regions.

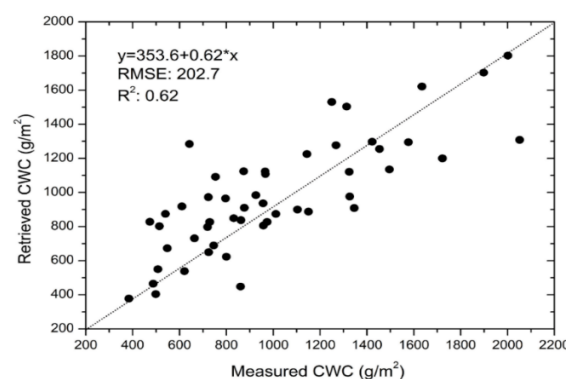


**Figure 5.** The scatterplot of the retrieved CWC *versus* ground-measured CWC.



## 4.2. Results of Validating GDI Using SPI

### 4.2.1. Downscaling AMSR-E Soil Moisture

Employing polynomial fitting, the data of NDVI and LST in both grassland regions and barren or sparsely vegetated regions were included in the regression model. Then, the aggregated NDVI, LST, and the AMSR-E data for 13 August over a period of 9 years (2002–2010) were used to estimate the regression model. Figure 6 shows the fitting results over the 9 years and Table 2 are the values of the correlation coefficient.

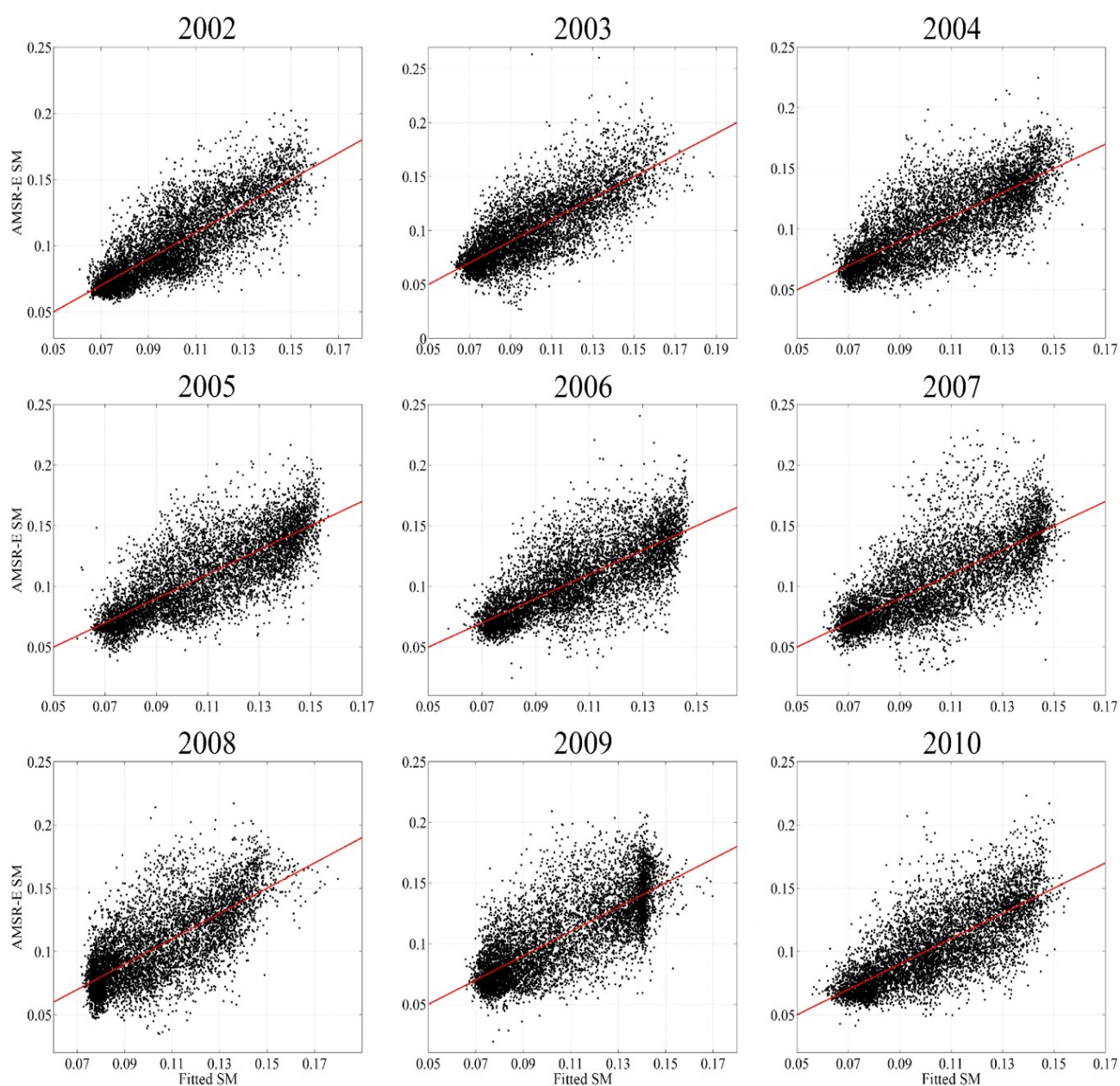


**Figure 6.** The scatterplots of the fitted SM *versus* the AMSR-E SM in August 2002–2010 in grassland regions and barren or sparsely vegetated regions in China.

According to fitting results, the fitted SM and the AMSR-E soil moisture data have good accordance for all of the years. The results are relatively poor in 2008 and 2009 in the considered regions, especially in areas with high values. However, the correlation coefficients (R) for all of the years are satisfactory, with an average R of 0.7668, and an average RMSE of 0.02 g/cm<sup>3</sup> for the 9 years.

**Table 2.** The fitting parameters of the scatterplots in Figure 6.

Years	Correlation Coefficient (R)	RMSE (g/cm <sup>3</sup> )
2002	0.8224	0.01614
2003	0.7832	0.01958
2004	0.7765	0.01959
2005	0.7807	0.0199
2006	0.7481	0.01986
2007	0.7416	0.02242
2008	0.7312	0.02101
2009	0.7625	0.02158
2010	0.7550	0.01952

#### 4.2.2. Validation Results

After eliminating the stations covered by clouds or reporting invalid data, we extracted data from approximately 350 stations during 2002–2010. In addition, the SDCI, which is constructed by integrating the scaled NDVI, LST and precipitation data, and the VHI was chosen as the comparison model. The correlation coefficients (R) were calculated for remote sensing parameters, which are the inputs of the drought indices and drought indices *versus* SPIs for the grassland regions of China. Tables 3 and 4 report the correlation results.

Table 3 shows that the scaled precipitation is highly related to SPI at all timescales. The scaled LST is more related to SPI than it is to the other land surface parameters, and the long-term SPI is relatively weakly related to the scaled LST, which indicates that the LST is sensitive to recent precipitation. However, the scaled NDVI and CWC have a higher correlation coefficient with the long-term SPI than with the 1-month SPI, which is in accordance with the phenomenon whereby vegetation responds to precipitation with a delay. According to the drought studies of Zhang [70], the relationship between the scaled NDVI and SPI varies considerably across different regions and different months. For arid regions with low vegetation density, the vegetation is substantially affected by the precipitation level. The scaled NDVI and scaled SM are highly correlated with the SPI. Regarding humid regions with high vegetation density, they consistently have a weak relationship with the SPI because vegetation that can obtain sufficient water in the absence of rainfall is affected by other factors. In our study areas, the scaled NDVI, CWC, and SM were weakly related to the SPI at all timescales. One of the reasons for this result is that some grassland areas in China are located in regions with high vegetation densities, thereby reducing the correlation. Another likely explanation is that rainfall affects a large region. A large part of the grass may be substantially affected by precipitation, but the small pixel size of 1 km in a region may introduce uncertainty. Precipitation is not the sole factor influencing the grass. Therefore, the SPI can effectively reflect a meteorological drought, which is defined as a lack of precipitation in a region over a given



period of time, but because the measure only considers precipitation, it is difficult to use SPI to monitor drought conditions on the land surface, especially at a high spatial resolution. To realize more comprehensive drought monitoring, ground information is necessary.

**Table 3.** The correlation coefficient (R) between the scaled remote sensing parameters and the *in situ* SPI at multiple timescales (1, 3, 6 and 9 month). TRMM-1, TRMM-3, and TRMM-6 represent the monthly, three-month, and six-month TRMM precipitation data.

Parameters	SPI-1 Mon	SPI-3 Mon	SPI-6 Mon	SPI-9 Mon
scaled CWC	0.12	0.12	0.15	0.14
scaled SM	0.15	0.17	0.10	0.11
scaled NDVI	0.14	0.20	0.20	0.20
scaled LST	0.31	0.24	0.23	0.24
scaled TRMM-1	<b>0.73</b>	0.46	0.41	0.41
scaled TRMM-3	0.43	<b>0.70</b>	0.63	0.62
scaled TRMM-6	0.39	0.62	<b>0.70</b>	<b>0.69</b>

**Table 4.** The correlation coefficient (R) between the drought indices and the *in situ* SPI at multiple timescales (1, 3, 6 and 9 months). TRMM-1, TRMM-3, and TRMM-6 represent the monthly, three-month, and six-month TRMM precipitation data used in the drought indices, respectively.

Drought Indices	SPI-1 Mon (TRMM-1)	SPI-3 Mon (TRMM-3)	SPI-6 Mon (TRMM-6)	SPI-9 Mon (TRMM-6)
GDI-1	0.54	0.53	0.51	0.51
GDI-2	<b>0.62</b>	<b>0.60</b>	<b>0.59</b>	<b>0.59</b>
GDI-3	0.49	0.49	0.48	0.47
SDCI	<b>0.64</b>	<b>0.61</b>	<b>0.61</b>	<b>0.61</b>
VHI	0.29	0.28	0.27	0.28

According to Table 4, GDI-1, GDI-2, GDI-3, and SDCI have strong correlations with the SPI, and the weight assigned to precipitation substantially affects the correlation coefficients. Following Rhee [5], we selected GDI2, which has the highest correlation values among the three weights used to construct GDI, as the final GDI algorithm. Therefore, the selected index with weights of  $1/2 \times PRE_{scaled} + 1/4 \times SM_{scaled} + 1/4 \times CWC_{scaled}$  was named GDI. In addition, the VHI measure proposed to represent the health of vegetation exhibited low correlation with the SPI. The SDCI has a little higher correlation to SPI than our GDI. The reason is that the NDVI and LST have a higher correlation coefficient than CWC and SM. In conclusion, GDI2 is somewhat correlated with the SPI and yields a similar result to that of SDCI.

### 4.3. Results of Validating the GDI Using USDM maps

#### 4.3.1. Downscaling AMSR-E Soil Moisture

Similar to the AMSR-E downscaling scheme in Section 4.2.2, we acquired soil moisture data for US regions at a 1 km resolution from the AMSR-E soil moisture data, the MODIS LST product, and NDVI

calculated based on land surface reflectance. The fitting results between AMSR-E soil moisture data and the soil moisture data reported by the regression model for the period 2002–2010 are shown in Figure 7.

Table 5 shows that the average correlation coefficient  $R$  is 0.5288, and that the average RMSE is  $0.02 \text{ g/cm}^3$  for the 9 years. The best fitting results are observed for 2002. However the correlations between the LST, NDVI and AMSR-E soil moisture data in the contiguous US are relatively lower than those in China. The fitted SM values are in accordance with those of the AMSR-E product.

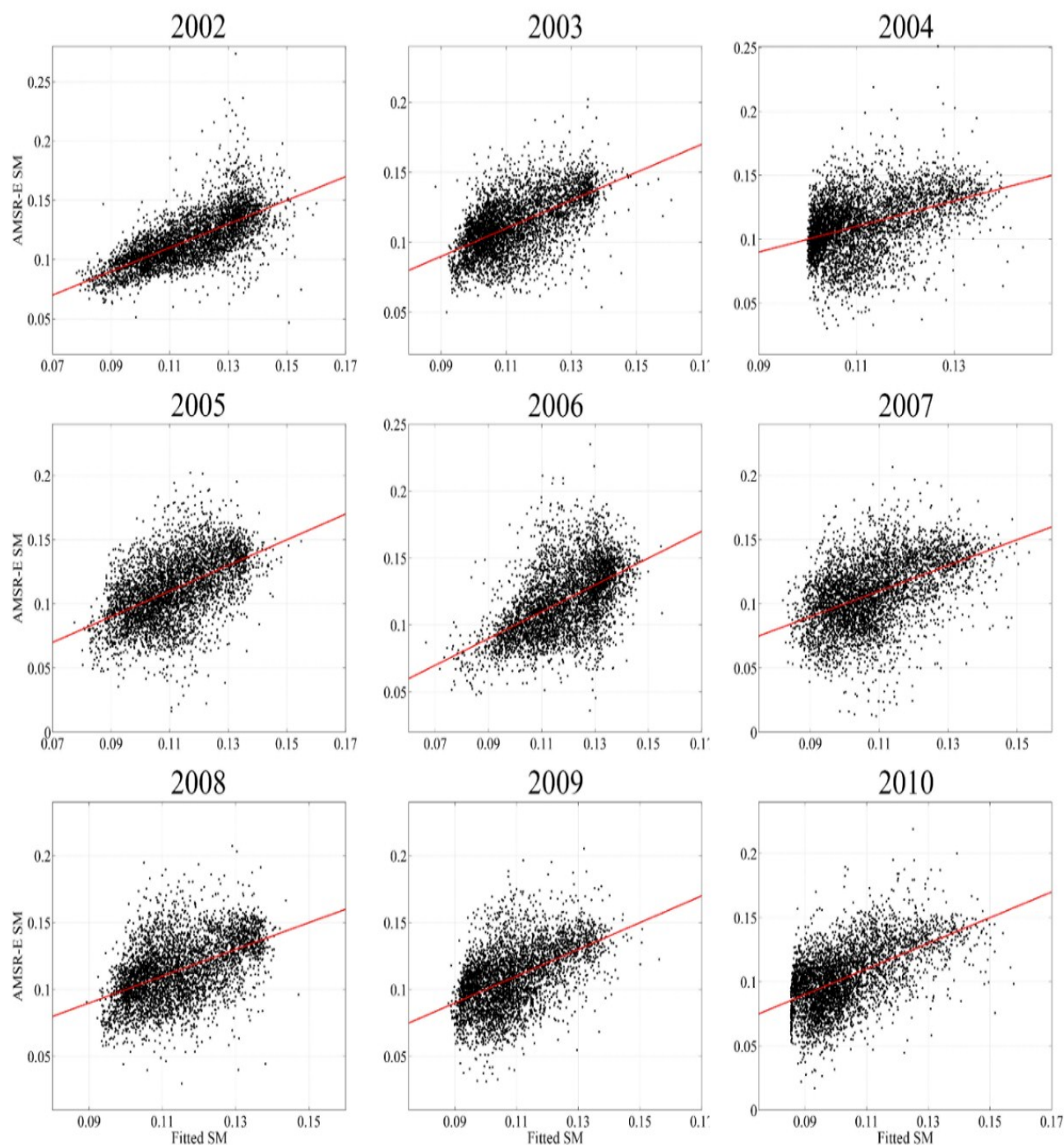


**Figure 7.** The scatterplots of the fitted SM *versus* the AMSR-E SM in August 2002–2010 in grassland regions and barren or sparsely vegetated regions of the contiguous US.

**Table 5.** The fitting parameters of the scatterplots in Figure 7.

Years	Correlation Coefficient (R)	RMSE (g/cm <sup>3</sup> )
2002	0.6885	0.01598
2003	0.5775	0.01658
2004	0.3999	0.02103
2005	0.5213	0.02146
2006	0.5394	0.02172
2007	0.4803	0.02298
2008	0.4905	0.02008
2009	0.5140	0.01996
2010	0.5477	0.02024

#### 4.3.2. Validation Results

USDM maps from August 2002–2009 were compared with the GDI maps. Because USDM maps are created on a weekly basis, maps for the end of the August were used for comparison. When constructing the GDI, we used three types of precipitation data aggregated at different timescales—TRMM-1, TRMM-3, and TRMM-6. The GDI was calculated using these different types of precipitation data to explore which precipitation timescale is appropriate. The GDI-1TRMM, GDI-3TRMM and GDI-6TRMM represent the GDI estimated by TRMM-1, TRMM-3 and TRMM-6, respectively, in the following comparison (Figure 8). Although GDI monitors drought only for grassland regions, all land cover types were included in the mapping for displaying purposes.

The GDI was classified into six classes and rendered in similar colors to those used in the USDM maps to permit more convenient visual comparison. The spatial distributions yielded by the GDI-1TRMM for the period 2002–2010 generally have relatively weak correlation with the spatial distributions in the USDM maps. However, for most of the years, the GDI-3TRMM and GDI-6TRMM generate satisfactory results when comparing their distributions to those of the USDM maps. In some regions, the GDI-3TRMM yields better results, but the GDI-6TRMM exhibits stronger overall correlation with the USDM maps. Therefore, the GDI based on 6-month accumulated precipitation data was chosen as the global product. In Section 4.4, this global product will be generated to monitor grassland drought at the global level.

In 2005, the GDI-1TRMM indicates a severer drought in the northwestern US, but it shows a satisfactory result in the bottom of the US maps. The GDI-3TRMM and GDI-6TRMM exhibit similar distributions to that of the USDM maps, and GDI-3TRMM is relatively more satisfactory. In 2006, the GDI-6TRMM has the best results among the three GDIs, but none of the GDIs were able to reflect the severe drought in the southern US. Our analysis reveals that the reason for this discrepancy is that the precipitation in the regions is in accordance with the USDM maps, but the SM in this region is relatively high compared with that of other years. In 2007, a severe drought occurred in California and contributed to extreme severity of the October 2007 wildfire in California. We can clearly observe that the GDI-6TRMM shows a severe drought in California. In addition, the drought in the southeastern US monitored by USDM is also captured by the GDIs, and the GDI-6TRMM shows the best results by comparison. In 2009, based on short term precipitation, the values of GDI-1TRMM appear too low in the southeastern US. The main drought occurs at the bottom of the USDM maps, and most of the other regions do not

suffer from drought. The GDI that is most related to the USDM maps, is the GDI-6TRMM. It successfully reflects the severe drought in the southernmost part of the US and agrees with USDM maps in other regions.

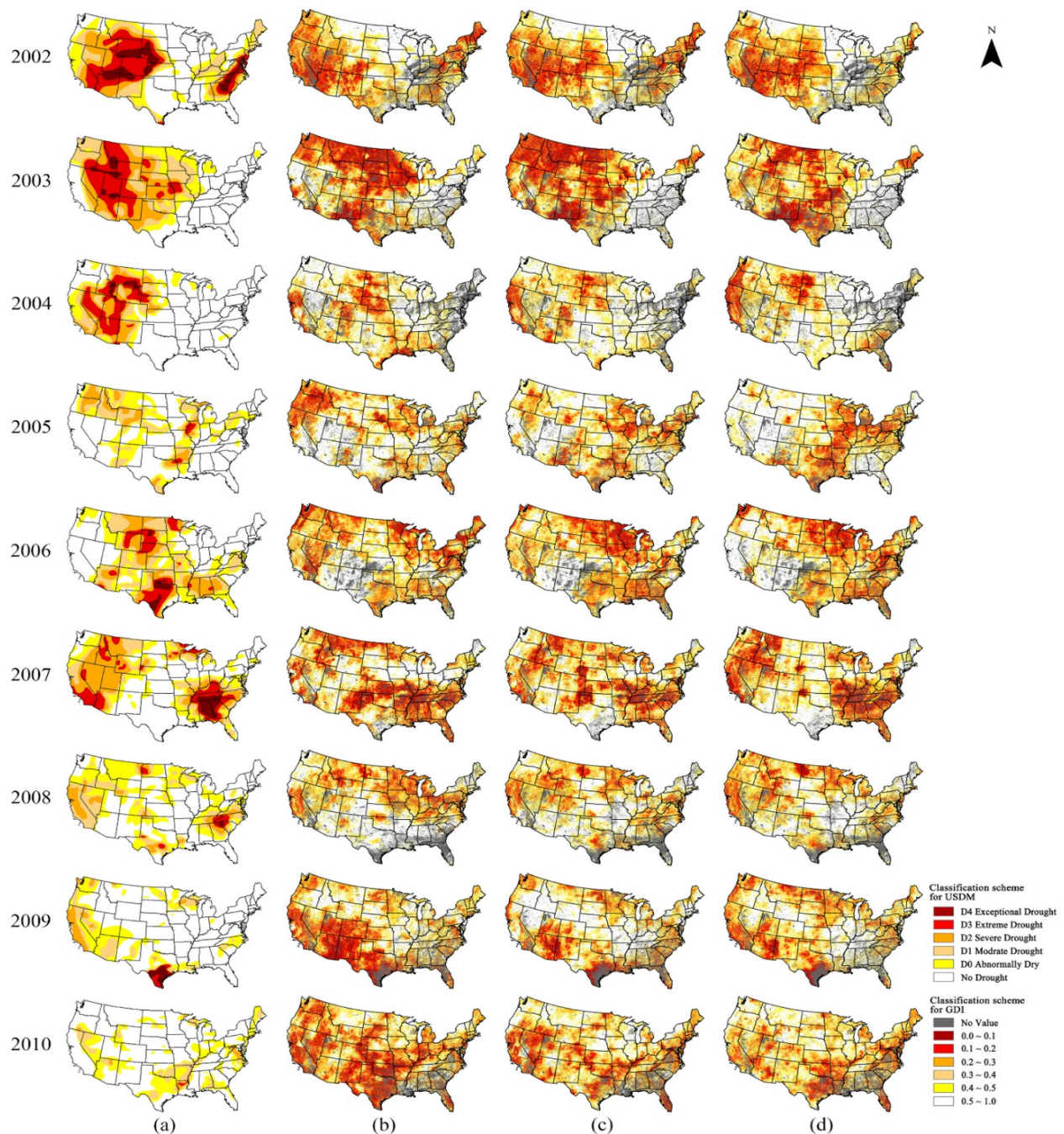


**Figure 8.** The spatial distribution of the drought indices for 2002–2010. (a) USDM; (b) GDI-1TRMM; (c) GDI-3TRMM; (d) GDI-6TRMM.

#### 4.4. Generating and Evaluating the Global GDI Product

In this section, the GDI-6CRU were calculated using six-month accumulated precipitation from CRU, and SPEI-6mon represents the SPEI at a time scale of six months. We ignored the regions with negative NDVI values because a negative NDVI value generally indicates that a region is covered by snow, cloud,



or water, which will cause errors in the estimation of EWT and SM. To test the performance of the GDI at the global scale, we quantitatively analyzed the spatial concordance between the global SPEI products and the global GDI products over the grassland regions, and the SPEI data were considered on a timescale of six months.

For simplicity, only the GDI and SPEI results for six months per year, including 2005, 2007, and 2009, are presented here. Based on a similar color-rendering scheme as that used for the SPEI, we can visually compare the performance of the GDI. According to month-to-month changes and spatial distributions depicted in Figures 9–11, the GDI has a similar spatial distribution to that of the SPEI and can capture most of the drought and wetness indicated by SPEI, and GDI has relatively smooth transition in the transitional zones between areas characterized by drought and wetness. The drought conditions over the contiguous US shown by SPEI are very similar to the GDI results for nearly all months during the three years considered. However, the GDI generally shows a severer and more extensive drought, especially for the east of South America in May, July, and September of 2007 and for southern Africa in 2005. The reason may be that the GDI estimation was obtained based on six years' of data, which is a short period compared with several decades. Thus, the ranges of values for precipitation, SM, and CWC were relatively narrow, which resulted in the polarization of the scaled parameters because the scaled parameters were calculated based on the range of their historical values, and thus generated drier and more humid results than those of SPEI. In Australia, the GDI shows a severe drought in March and May 2005, and January and September 2007, while the SPEI shows that the regions suffering from a mild drought. The reason for this disparity is the extreme low scaled precipitation values extracted by CRU. In addition, the drought conditions in Australia that were aggravated from January to November 2009 are successfully monitored by the GDI. In Africa, the drought distribution produced by the GDI is highly concordant with the SPEI results for 2009, but they differ in the severity of the droughts. For northern China, the droughts monitored by SPEI in the three years considered are well identified by the GDI.

The categories of the SPEI were obtained from the SPEI Global Drought Monitor. However, the categories in the GDI maps were not determined based on an in-depth investigation but arbitrarily classified for display purposes, which will also cause visual errors. Therefore, more meaningful break points for the GDI values should be found for the scientific display of the drought scale in further work.

To conduct a further evaluation about the performance of the global GDI product, we investigated the drought events happening during 2005–2010 and recorded their location and date of occurrence. Four severe drought events were chosen, and were introduced in following. Though SPEI is in a coarse spatial resolution of 0.5 degree (approximate 55 km), to make an easy comparison between GDI and SPEI, SPEI in grassland regions was extracted also based on the 1-km land cover types.

In 2006–2007, a severe drought occurred in California, US, and contributed to the extreme severity of the 2007 California wildfires. According to Figure 12, GDI captures this severe drought and shows that the drought started in the October 2006, and didn't weaken until October 2007. SPEI presents a similar development tendency of the drought in the period.

In 2008 and 2009, much of south and south-central Texas, US, were in a state of exceptional drought. According to Figure 13, GDI shows that Texas suffered a drought throughout August 2008 to August 2009, but the SPEI shows that the drought started in February 2009, which is later than the occurrence time of the drought event.

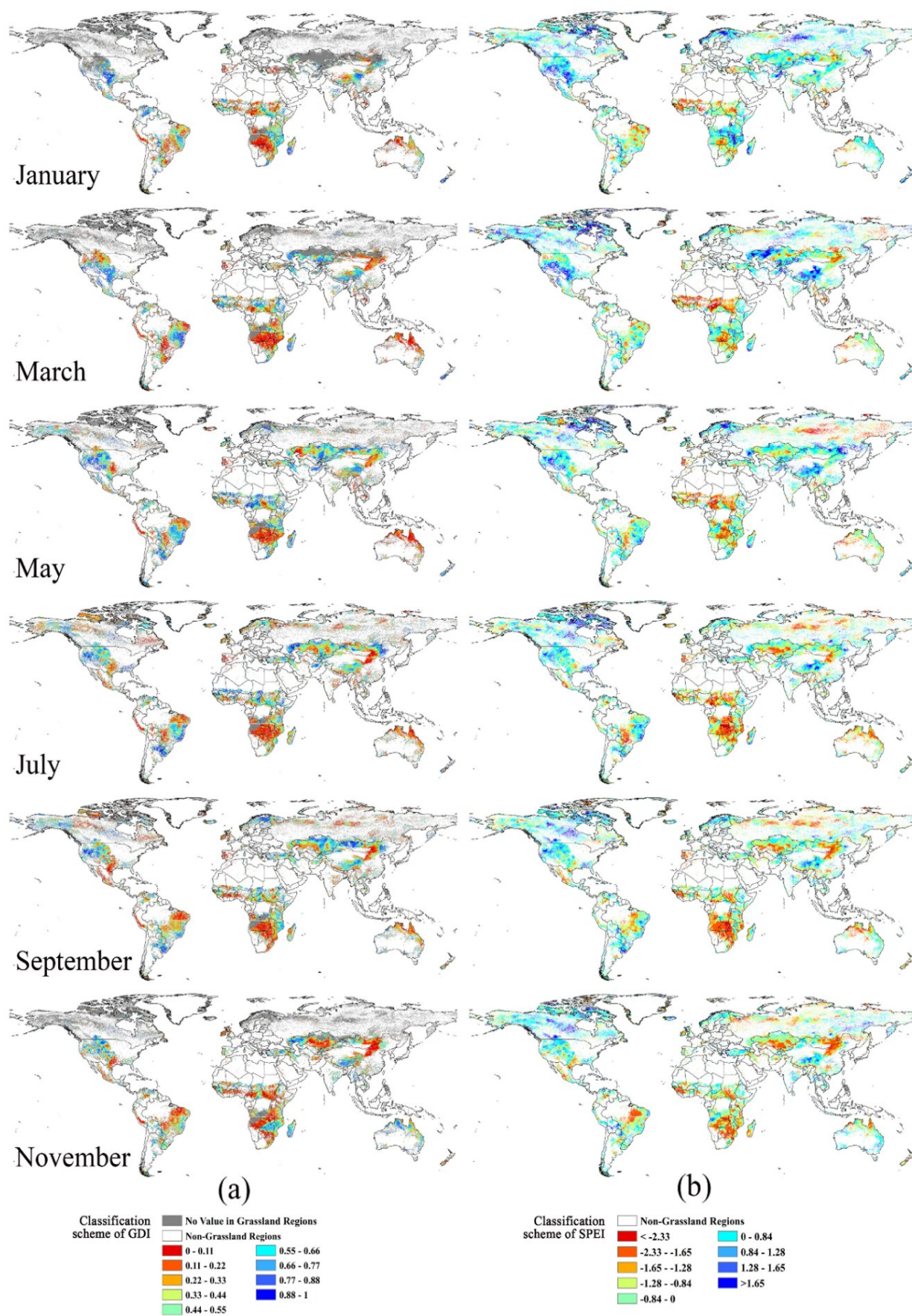


**Figure 9.** The global distribution of the GDI-6CRU and SPEI-6mon for grassland regions in different months of 2005. (a) GDI-6CRU; (b) SPEI-6mon.



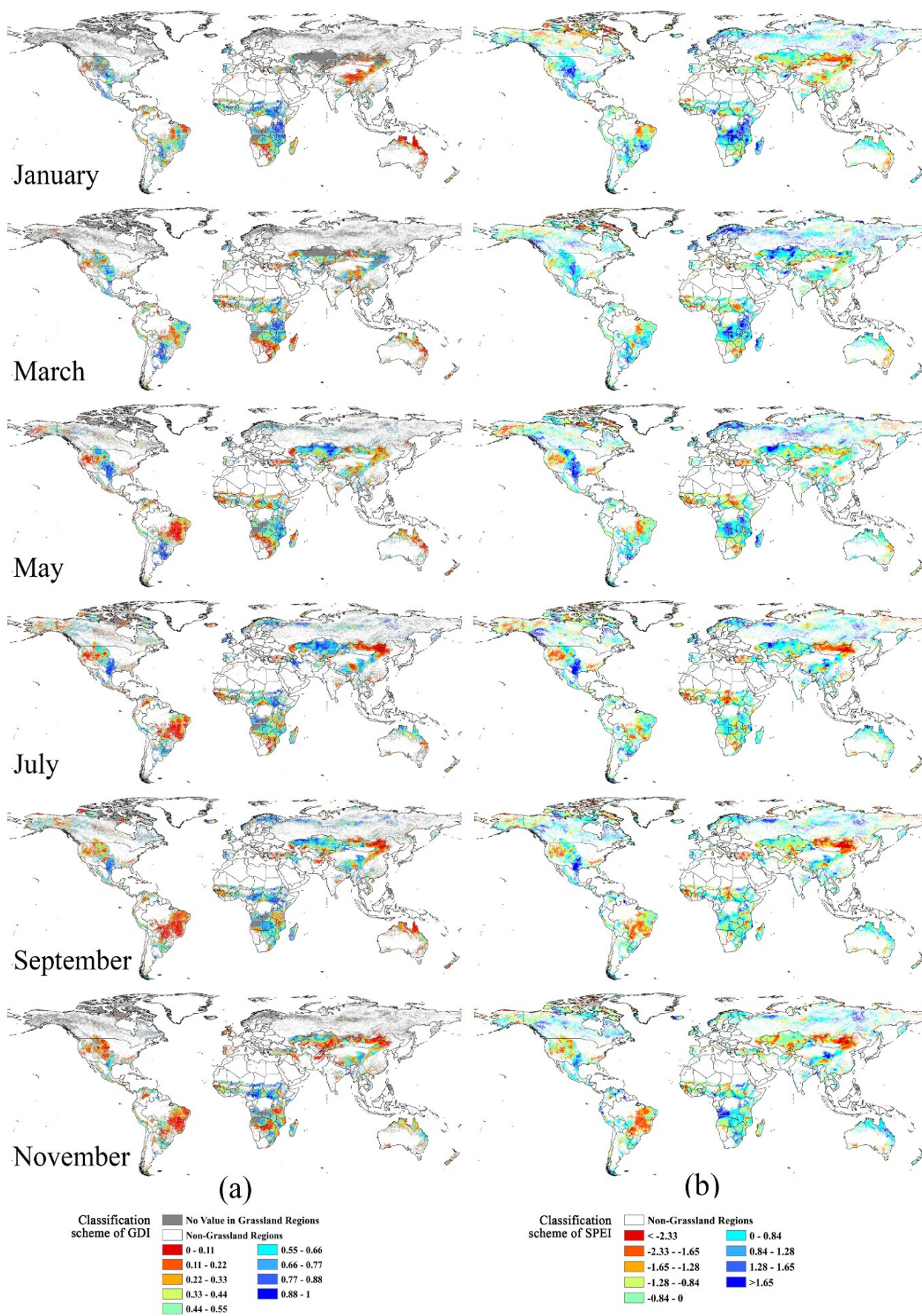


**Figure 10.** The global distribution of the GDI-6CRU and SPEI-6mon for grassland regions in different months of 2007. (a) GDI-6CRU; (b) SPEI-6mon.



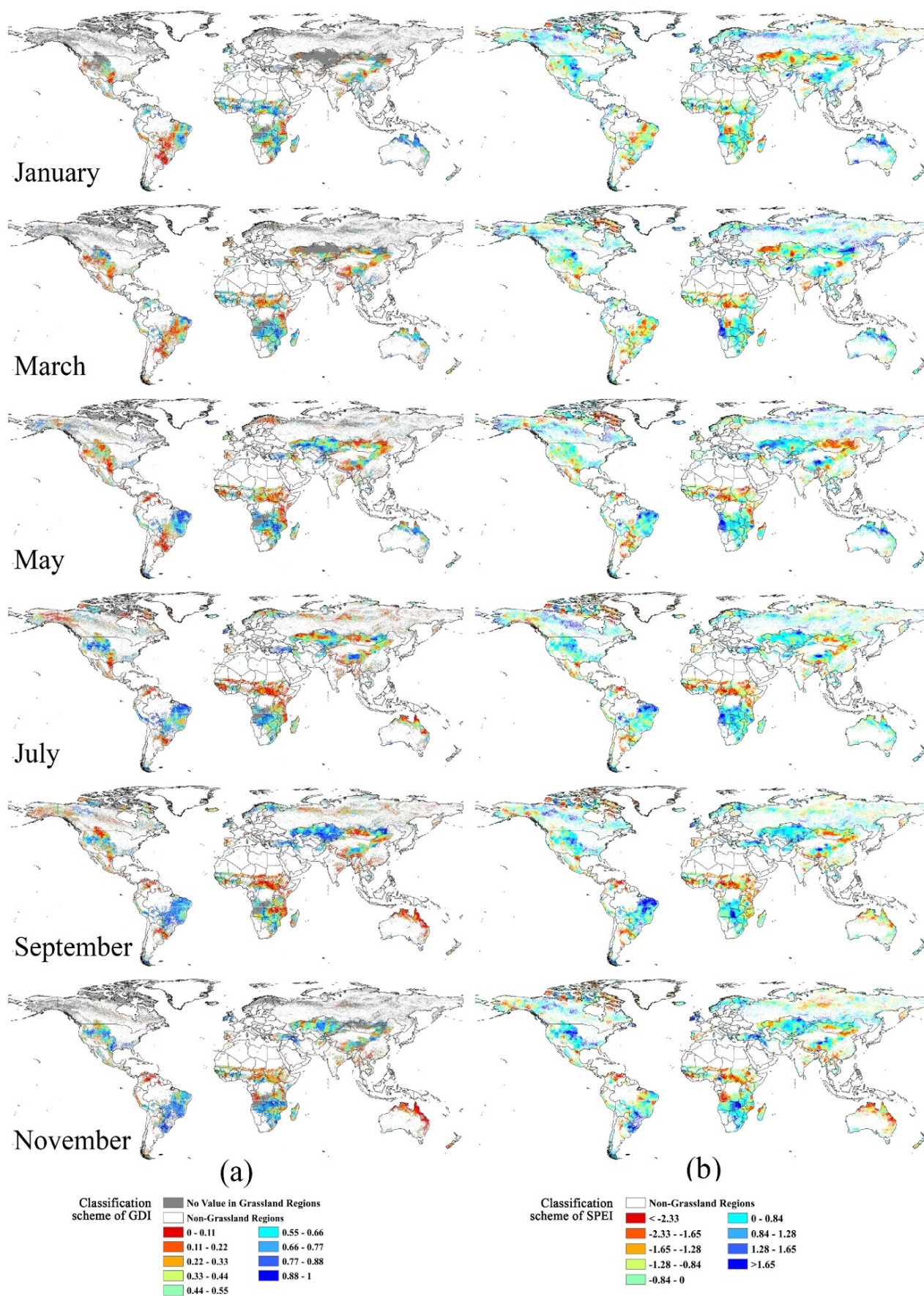


**Figure 11.** The global distribution of the GDI-6CRU and SPEI-6mon for grassland regions in different months of 2009. (a) GDI-6CRU; (b) SPEI-6mon.



During the summer of 2006, Sichuan Province and Chongqing Municipality, experienced their most severe drought during the last 50 years. According to Figure 14, both GDI and SPEI indicate that the drought started in summer of 2006, and GDI shows the drought attenuated in December, but SPEI shows the drought get worsen in December. Therefore, GDI gets a relative satisfied result because it agrees with the drought events that this severe drought lasted in the summer of 2006, and it clearly reflects the change of the drought.

In spring 2010, large areas of Southwest China were hit by a long-lasting and severe drought. The drought started in autumn of 2009 and sustained until April 2010 [72]. According to Figure 15, GDI shows that the drought started in September 2009, and deteriorated in the following months until to April 2010. The drought changing time showed by GDI agree quite well with the investigated drought event. SPEI shows that the drought became obvious in October 2009. This agrees with that the drought started in autumn of 2009, but SPEI shows that there are little drought in April, 2010 when the drought actually did not end. Moreover, according to SPEI, Yunnan which is one of the largest victims suffered a more moderate drought than the results shown by GDI.

According to the above comparison based on the four drought events, GDI captured the location and the variation time and trend of the drought. SPEI also captured the drought, but there were some undesirability when monitoring the time of drought changing. Moreover, GDI in a spatial resolution of 1 km provided much more detailed information about the drought than SPEI which is in a spatial resolution of 0.5°.

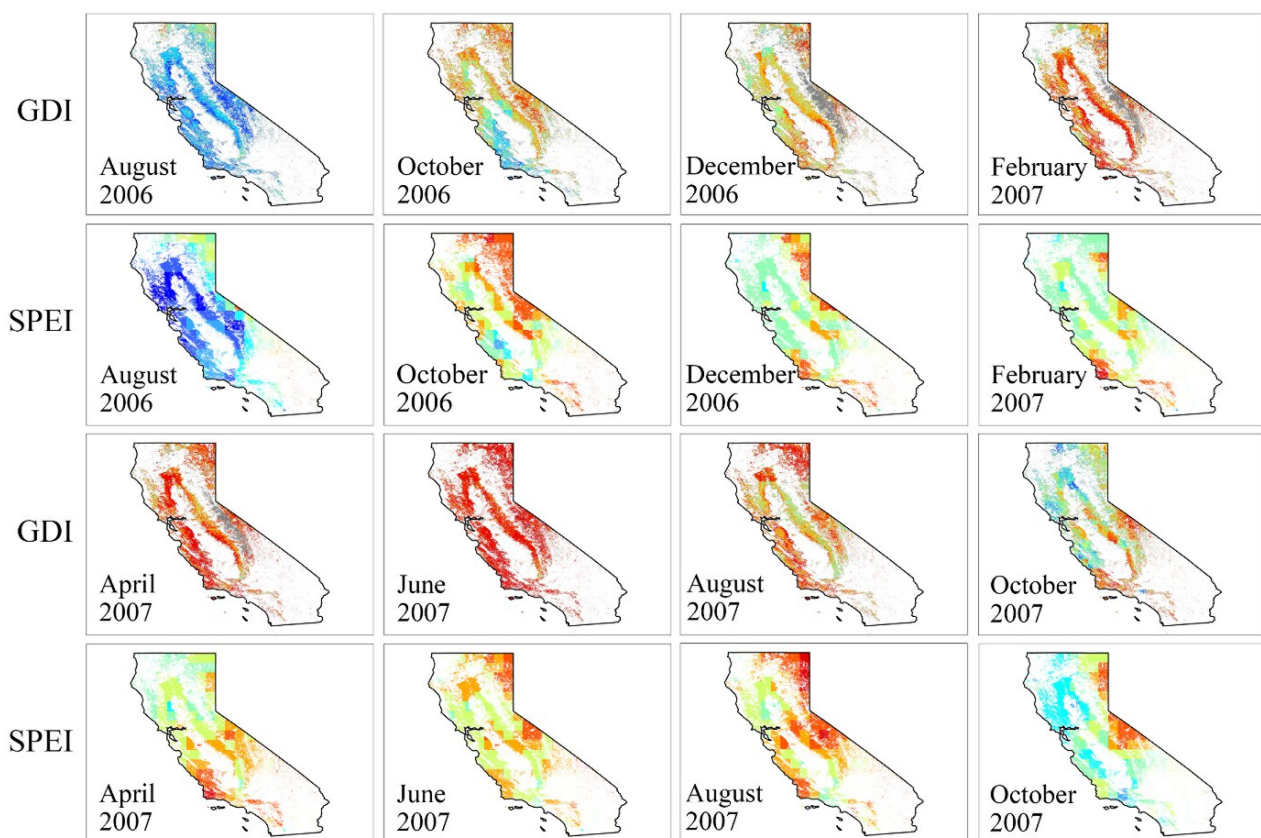


**Figure 12.** The performance of the GDI-6CRU and SPEI-6mon in grassland regions, regarding the drought event in 2006–2007, California, US. The classification scheme of GDI-6CRU and SPEI SPEI-6mon are same with the scheme adopted in Figures 9–11.

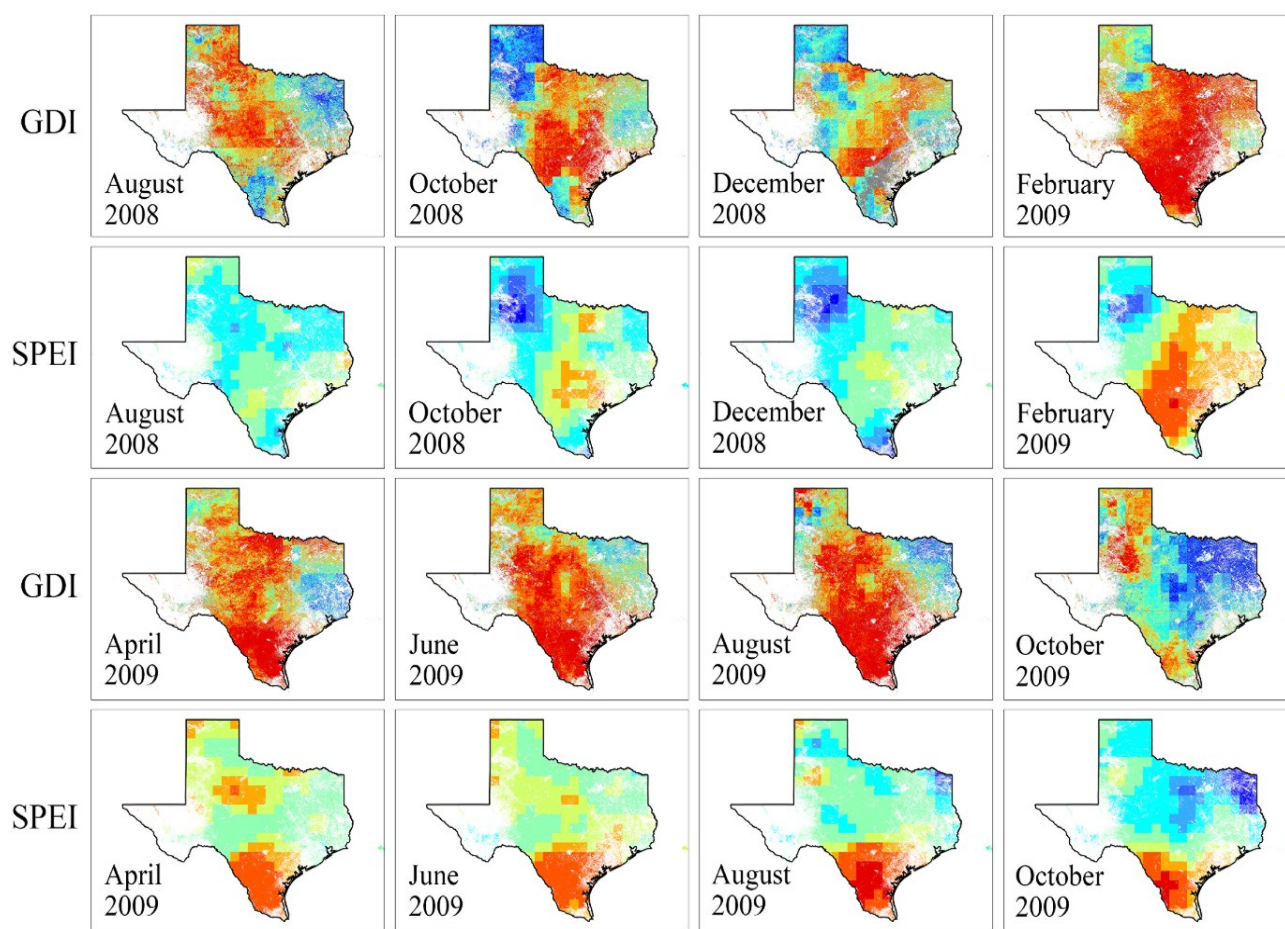


**Figure 13.** The performance of the global products of GDI-6CRU and SPEI-6mon in grassland regions, regarding the drought event in 2008 and 2009, Texas, US. The classification scheme of GDI-6CRU and SPEI SPEI-6mon are same with the scheme adopted in Figures 9–11.

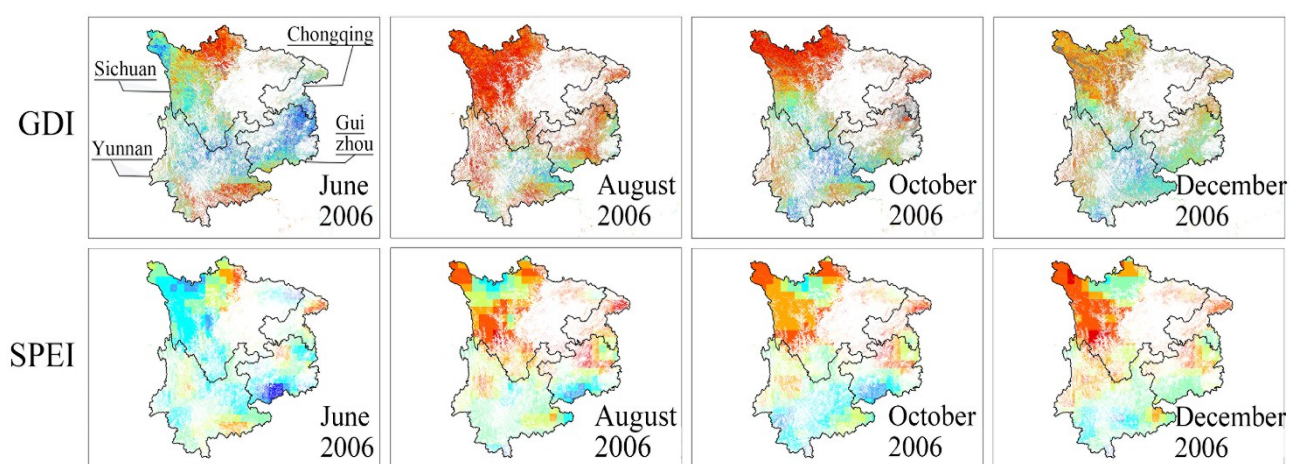


**Figure 14.** The performance of the global products of GDI-6CRU and SPEI-6mon in grassland regions, regarding the drought event in summer of 2006, Southwest China. The classification scheme of GDI-6CRU and SPEI SPEI-6mon are same with the scheme adopted in Figures 9–11.



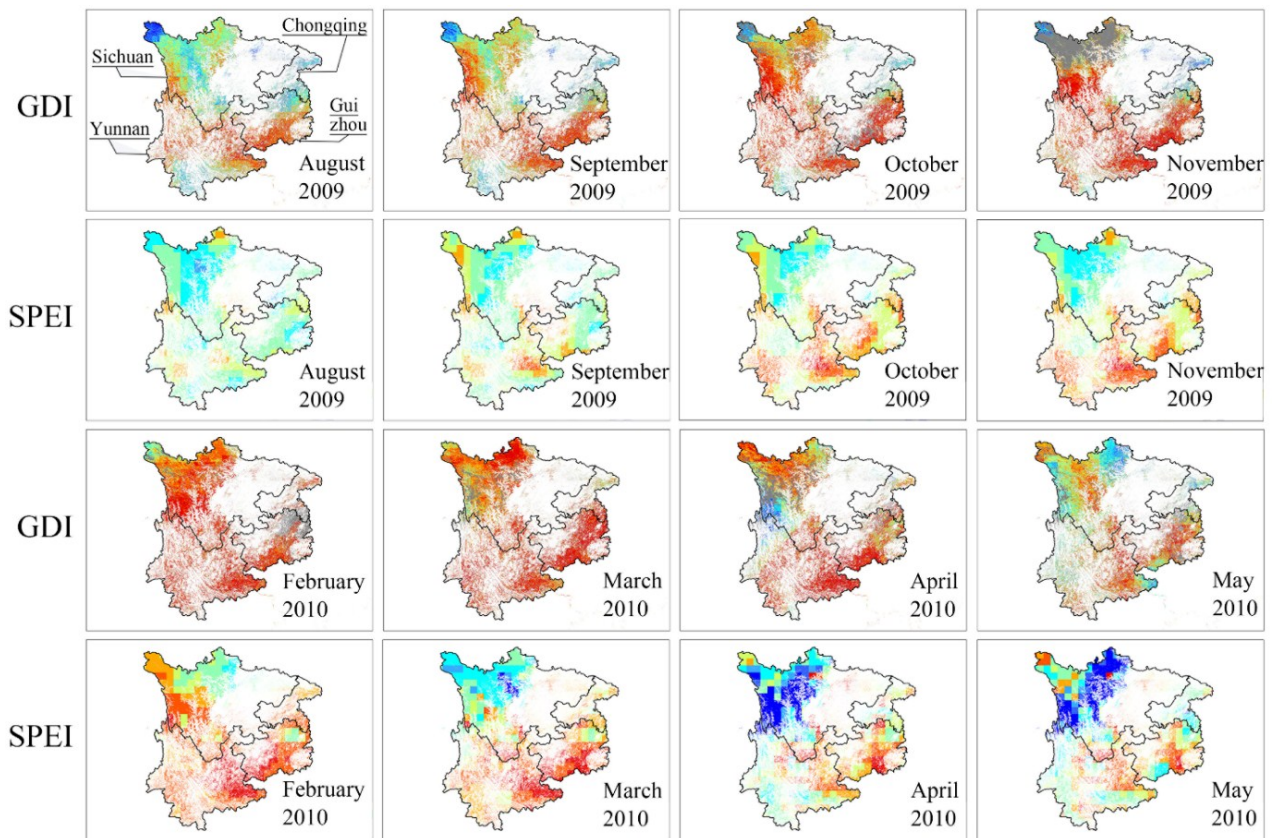


**Figure 15.** The performance of the global products of GDI-6CRU and SPEI-6mon in grassland regions, regarding the drought event in 2010, Southwest China. The classification scheme of GDI-6CRU and SPEI-6mon are same with the scheme adopted in Figures 9–11.

## 5. Conclusions

This study proposed a new index, called the GDI, for drought monitoring in grassland ecosystems. Based on the analysis of the water cycle in grasslands, we selected precipitation, CWC, and SM as input indicators to estimate the water conditions in the air, vegetation, and soil layers, respectively. Because the monitoring object of the GDI is the grassland, which is horizontally homogeneous, the PROSAI model was employed to estimate the CWC. The SM downscaling method was used to generate the SM at a 1 km scale, and the precipitation data were directly obtained from existing precipitation data. The GDI was constructed by combining the three indicators, which were scaled from 0 to 1 based on their historical values. By analyzing the correlation between the GDI and the SPI, we determined the weights of the three indicators and completed the construction of the GDI.

According to the validation using the *in situ* SPI at the regional scale, the results showed that the GDI was in accordance with the SPI and had a similar performance to that of the SDCI. The correlation coefficients between the SPI and GDI are approximately 0.6. In addition, most ground information were weakly related to the SPI with the correlation coefficient less than 0.3, which means that it would be difficult to monitor the drought condition of the ground based solely on precipitation data. Regarding the comparison between the GDI and USDM maps, the GDI combined with the TRMM-6 exhibited satisfactory drought-monitoring performance and agreed well with the USDM for most of the years considered. The global GDI successfully captured most of the drought and wetness identified by the

SPEI, but there were some differences concerning drought severity. In addition, according to the further evaluation about the global GDI product using the four happened drought events, GDI well captured the location and the variation time and trend of the drought, and it provided much more detailed information about the drought that SPEI thanks to its high spatial resolution of 1 km.

Because the innovation of GDI is its comprehensive drought monitoring through the integration of CWC, SM, and precipitation data, the algorithm for estimating these indicators can be optimized or replaced. There are several limitations of GDI which can be optimized. (1) The weights assigned to the precipitation, CWC, and SM variables in our study may not be suitable for all regions, and they can be adjusted for different purposes and regions. For example, if the study focuses more on the drought impacts on land surface, the weights of CWC and SM can be increased; (2) The parameters used in PROSAIL model to estimate CWC were based on a general condition of grassland. To reach a more accurate estimation in a certain region, the parameters can be optimized based on the *priori* knowledge of the local ecosystem conditions. Moreover, the large spatial heterogeneity of vegetation might affects the estimation of CWC; (3) The uncertainties of 1-km SM will increase in regions where SM is weakly correlated with vegetation and temperature, because the variability of 1-km SM is described primarily by the vegetation index and LST changes. The downscaling methods was employed in the study for its simplicity and easy availability of the necessary inputs while generating global products, but a more suitable method that can better capture the variability of 1-km soil moisture can be adopted if the study is at regional scale; (4) The temporal coverage of the data used to generate global product was six years, using data with a longer temporal coverage will help for a more accurate estimation about drought and its impacts. Though there are a few limitations that can be optimized, the methods and model parameters used in the study can provide a valuable reference for drought monitoring. The regional validation section in this study was based solely on data from August, which is during the growing season for our regions. We did not explore the drought effects caused by different seasons in detail; but we roughly compared the global GDI with the global SPEI in different months. In our next work, we will conduct a more comprehensive study of drought effects in different months.

## Acknowledgments

This work was supported by the National High-Tech Research and Development Program of China (Contract No. 2013AA12A302), the Fundamental Research Fund for the Central Universities (Contract No. ZYGX2012Z005), and the National Natural Science Foundation of China (Contract No. 41471293). The authors sincerely thank Yu Zhu, Dasong XU, Qian Feng, Xueting Zhang and Qianqian Yuan for the data processing and Yang Jun for the revision.

## Author Contributions

The idea was conceived by Binbin He, Zhanmang Liao and Xingwen Quan, performed by Zhanmang Liao and Junjie Hu, analyzed by Zhanmang Liao, Binbin He, Xingwen Quan and Xing Li, written by Zhanmang Liao, and revised by Xing Li and Xingwen Quan.

## Conflicts of Interest

The authors declare no conflict of interest.

## References

1. Wilhite, D.A. Drought as a natural hazard: Concepts and definitions. *Drought Glob. Assess.* **2000**, *1*, 3–18.
2. Svoboda, M.; LeCompte, D.; Hayes, M.; Heim, R.; Gleason, K.; Angel, J.; Rippey, B.; Tinker, R.; Palecki, M.; Stooksbury, D. The drought monitor. *Bull. Am. Meteorol. Soc.* **2002**, *83*, 1181–1190.
3. Conner, R.; Siedl, A.; Tassell, L. USA Grasslands and Related Resources: An Economic and Biological Trends Assessment. Available online: <http://irnr.tamu.edu/publications/research-reports/2001/united-states-grasslands-and-related-resources-an-economic-and-biological-trends-assessment/> (accessed on 24 September 2015).
4. Caccamo, G.; Chisholm, L.; Bradstock, R.A.; Puotinen, M. Assessing the sensitivity of MODIS to monitor drought in high biomass ecosystems. *Remote Sens. Environ.* **2011**, *115*, 2626–2639.
5. Rhee, J.; Im, J.; Carbone, G.J. Monitoring agricultural drought for arid and humid regions using multi-sensor remote sensing data. *Remote Sens. Environ.* **2010**, *114*, 2875–2887.
6. Heim, R.R., Jr. A review of twentieth-century drought indices used in the United States. *Bull. Am. Meteorol. Soc.* **2002**, *83*, 1149–1165.
7. Tucker, C.J.; Choudhury, B.J. Satellite remote sensing of drought conditions. *Remote Sens. Environ.* **1987**, *23*, 243–251.
8. Bayarjargal, Y.; Karnieli, A.; Bayasgalan, M.; Khudulmur, S.; Gandush, C.; Tucker, C. A comparative study of NOAA-AVHRR derived drought indices using change vector analysis. *Remote Sens. Environ.* **2006**, *105*, 9–22.
9. Ji, L.; Peters, A.J. Assessing vegetation response to drought in the Northern Great Plains using vegetation and drought indices. *Remote Sens. Environ.* **2003**, *87*, 85–98.
10. AghaKouchak, A.; Farahmand, A.; Melton, F.; Teixeira, J.; Anderson, M.; Wardlow, B.; Hain, C. Remote sensing of drought: Progress, challenges and opportunities. *Rev. Geophys.* **2015**, *53*, 452–480.
11. Wood, A.W. The University of Washington Surface Water Monitor: An Experimental Platform for National Hydrologic Assessment and Prediction. In Proceedings of American Meteorology Society annual meeting, 22nd conference on hydrology, New Orleans, LA, USA, 20–24 January 2008.
12. Wood, A.W.; Lettenmaier, D.P. A test bed for new seasonal hydrologic forecasting approaches in the western United States. *Bull. Am. Meteorol. Soc.* **2006**, *87*, 1699–1712.
13. Hao, Z.; AghaKouchak, A.; Nakhjiri, N.; Farahmand, A. Global integrated drought monitoring and prediction system. *Sci. Data* **2014**, *1*, doi:10.1038/sdata.2014.1.
14. Lyon, B.; Bell, M.A.; Tippet, M.K.; Kumar, A.; Hoerling, M.P.; Quan, X.-W.; Wang, H. Baseline probabilities for the seasonal prediction of meteorological drought. *J. Appl. Meteorol. Climatol.* **2012**, *51*, 1222–1237.

15. Vicente-Serrano, S.M.; Cabello, D.; Tomás-Burguera, M.; Martín-Hernández, N.; Beguería, S.; Azorin-Molina, C.; El Kenawy, A. Drought variability and land degradation in semiarid regions: Assessment using remote sensing data and drought indices (1982–2011). *Remote Sens.* **2015**, *7*, 4391–4423.
16. Palmer, W.C. *Meteorological Drought*; Department of Commerce, Weather Bureau: Washington, DC, USA, 1965.
17. Hayes, M.J.; Svoboda, M.D.; Wilhite, D.A.; Vanyarkho, O.V. Monitoring the 1996 drought using the standardized precipitation index. *Bull. Am. Meteorol. Soc.* **1999**, *80*, 429–438.
18. Heddinghaus, T.R.; Sabol, P. A review of the palmer drought severity index and where do we go from here. In Proceedings of the Seventh Conference on Applied Climatology, Boston, MA, USA, 10–13 September 1991.
19. McKee, T.B.; Doesken, N.J.; Kleist, J. The relationship of drought frequency and duration to time scales. In Proceedings of the 8th Conference on Applied Climatology, Boston, MA, USA, 17–22 January 1993; pp. 179–183.
20. Guttman, N.B. Accepting the Standardized Precipitation Index: A Calculation Algorithm. *J. Am. Water Res. Assoc.* **1999**, *35*, 311–322.
21. Vicente-Serrano, S.M.; Beguería, S.; López-Moreno, J.I. A multiscalar drought index sensitive to global warming: The standardized precipitation evapotranspiration index. *J. Clim.* **2010**, *23*, 1696–1718.
22. Tucker, C.J. Red and photographic infrared linear combinations for monitoring vegetation. *Remote Sens. Environ.* **1979**, *8*, 127–150.
23. Huete, A.; Liu, H.; Batchily, K.; Van Leeuwen, W. A comparison of vegetation indices over a global set of TM images for EOS-MODIS. *Remote Sens. Environ.* **1997**, *59*, 440–451.
24. Hunt, E.R., Jr.; Rock, B.N. Detection of changes in leaf water content using near-and middle-infrared reflectances. *Remote Sens. Environ.* **1989**, *30*, 43–54.
25. Claudio, H.C.; Cheng, Y.; Fuentes, D.A.; Gamon, J.A.; Luo, H.; Oechel, W.; Qiu, H.-L.; Rahman, A.F.; Sims, D.A. Monitoring drought effects on vegetation water content and fluxes in chaparral with the 970 nm water band index. *Remote Sens. Environ.* **2006**, *103*, 304–311.
26. Farrar, T.; Nicholson, S.; Lare, A. The influence of soil type on the relationships between NDVI, rainfall, and soil moisture in semiarid Botswana. II. NDVI response to soil moisture. *Remote Sens. Environ.* **1994**, *50*, 121–133.
27. Wang, J.; Price, K.; Rich, P. Spatial patterns of NDVI in response to precipitation and temperature in the central Great Plains. *Int. J. Remote Sens.* **2001**, *22*, 3827–3844.
28. Brown, J.F.; Wardlow, B.D.; Tadesse, T.; Hayes, M.J.; Reed, B.C. The vegetation drought response index (VegDRI): A new integrated approach for monitoring drought stress in vegetation. *GISci. Remote Sens.* **2008**, *45*, 16–46.
29. Park, S.; Feddema, J.J.; Egbert, S.L. Impacts of hydrologic soil properties on drought detection with MODIS thermal data. *Remote Sens. Environ.* **2004**, *89*, 53–62.
30. Kogan, F. Application of vegetation index and brightness temperature for drought detection. *Adv. Sp. Res.* **1995**, *15*, 91–100.
31. McVicar, T.; Bierwirth, P. Rapidly assessing the 1997 drought in Papua New Guinea using composite AVHRR imagery. *Int. J. Remote Sens.* **2001**, *22*, 2109–2128.

32. Narasimhan, B.; Srinivasan, R. Development and evaluation of soil moisture deficit index (SMDI) and evapotranspiration deficit index (ETDI) for agricultural drought monitoring. *Agr. For. Meteorol.* **2005**, *133*, 69–88.
33. Sandholt, I.; Rasmussen, K.; Andersen, J. A simple interpretation of the surface temperature/vegetation index space for assessment of surface moisture status. *Remote Sens. Environ.* **2002**, *79*, 213–224.
34. Gao, Z.; Gao, W.; Chang, N.-B. Integrating temperature vegetation dryness index (TVDI) and regional water stress index (RWSI) for drought assessment with the aid of Landsat TM/ETM+ images. *Int. J. Appl. Earth Obs. Geoinform.* **2011**, *13*, 495–503.
35. Kogan, F. World droughts in the new millennium from AVHRR-based vegetation health indices. *Eos Trans. Am. Geophys. Union* **2002**, *83*, 557–563.
36. Kogan, F.; Gitelson, A.; Zakarin, E.; Spivak, L.; Lebed, L. AVHRR-based spectral vegetation index for quantitative assessment of vegetation state and productivity. *Photogramm. Eng. Remote Sens.* **2003**, *69*, 899–906.
37. Liu, W.; Kogan, F. Monitoring brazilian soybean production using NOAA/AVHRR based vegetation condition indices. *Int. J. Remote Sens.* **2002**, *23*, 1161–1179.
38. Abbas, S.; Nichol, J.E.; Qamer, F.M.; Xu, J. Characterization of drought development through remote sensing: A case study in central Yunnan, China. *Remote Sens.* **2014**, *6*, 4998–5018.
39. Lloyd-Hughes, B.; Saunders, M.A. A drought climatology for Europe. *Int. J. Clim.* **2002**, *22*, 1571–1592.
40. Wu, H.; Hayes, M.J.; Weiss, A.; Hu, Q. An evaluation of the standardized precipitation index, the China-z index and the statistical z-score. *Int. J. Clim.* **2001**, *21*, 745–758.
41. China Meteorological Data Sharing Service System. Available online: <http://cdc.nmic.cn/home.do> (accessed on 2 March 2015).
42. Level 1 and Atmosphere Archive and Distribution System. Available online: <http://ladsweb.nascom.nasa.gov/> (accessed on 3 April 2015).
43. National Snow and Ice Data Center. Available online: <http://nsidc.org/> (accessed on 8 April 2015).
44. Njoku, E.G.; Jackson, T.J.; Lakshmi, V.; Chan, T.K.; Nghiem, S.V. Soil moisture retrieval from AMSR-E. *IEEE Trans. Geos. Remote Sens.* **2003**, *41*, 215–229.
45. Njoku, E.G. *AMSR-E/Aqua Daily L3 Surface Soil Moisture, Interpretive Parameters, and QC EASE-Grids V002*; National Snow and Ice Data Center: Boulder, CO, USA, 2008.
46. Rodell, M.; Beaudoing, H.K. *GLDAS Noah Land Surface Model l4 Monthly 0.25 × 0.25 Degree Version 2.0*; Goddard Earth Sciences Data and Information Services Center: Greenbelt, MD, USA, 2013.
47. Hualan Rui, H.B. Readme Document for Global Land Data Assimilation System, 2nd. Available online: <http://disc.sci.gsfc.nasa.gov/services/grads-gds/gldas> (accessed on 23 September 2015).
48. Goddard Earth Sciences Data and Information Services Center. Available online: <http://disc.sci.gsfc.nasa.gov/> (accessed on 14 July 2015).
49. Climate Research Unit. Available online: <http://www.cru.uea.ac.uk/> (accessed on 1 January 2015).
50. SPEI Global Drought Monitor. Available online: <http://sac.csic.es/spei/index.html> (accessed on 11 June 2015).

51. Vicente-Serrano, S.M.; Beguería, S.; López-Moreno, J.I.; Angulo, M.; El Kenawy, A. A new global 0.5 gridded dataset (1901–2006) of a multiscalar drought index: Comparison with current drought index datasets based on the palmer drought severity index. *J. Hydrometeorol.* **2010**, *11*, 1033–1043.
52. Thornthwaite, C.W. An approach toward a rational classification of climate. *Geogr. Rev.* **1948**, *66*, 55–94.
53. US Drought Monitor. Available online: <http://droughtmonitor.unl.edu/> (accessed on 29 April 2015).
54. Bonan, G.B. *Ecological Climatology: Concepts and Applications*; Cambridge University Press: Cambridge, UK, 2002.
55. Quan, X.; He, B.; Li, X.; Tang, Z. Estimation of grassland live fuel moisture content from ratio of canopy water content and foliage dry biomass. *IEEE Geosci. Remote Sens. Lett.* **2015**, *12*, 1903–1907.
56. Quan, X.; He, B.; Li, X. A Bayesian network-based method to alleviate the ill-posed inverse problem: A case study on leaf area index and canopy water content retrieval. *IEEE Trans. Geosci. Remote Sens.* **2015**, *53*, 6507–6517.
57. Verhoef, W. Light scattering by leaf layers with application to canopy reflectance modeling: The sail model. *Remote Sens. Environ.* **1984**, *16*, 125–141.
58. Jacquemoud, S.; Baret, F. Prospect: A model of leaf optical properties spectra. *Remote Sens. Environ.* **1990**, *34*, 75–91.
59. Jacquemoud, S.; Verhoef, W.; Baret, F.; Bacour, C.; Zarco-Tejada, P.J.; Asner, G.P.; François, C.; Ustin, S.L. Prospect+ sail models: A review of use for vegetation characterization. *Remote Sens. Environ.* **2009**, *113*, S56–S66.
60. Jacquemoud, S. Inversion of the prospect+ sail canopy reflectance model from AVIRIS equivalent spectra: Theoretical study. *Remote Sens. Environ.* **1993**, *44*, 281–292.
61. Institute de Physique du Globe de Paris. Available online: <http://teledetection.ipgp.jussieu.fr/prosail/> (accessed on 29 April 2015).
62. Jurdao, S.; Yebra, M.; Guerschman, J.P.; Chuvieco, E. Regional estimation of woodland moisture content by inverting radiative transfer models. *Remote Sens. Environ.* **2013**, *132*, 59–70.
63. Sow, M.; Mbow, C.; Hély, C.; Fensholt, R.; Sambou, B. Estimation of herbaceous fuel moisture content using vegetation indices and land surface temperature from MODIS data. *Remote Sens.* **2013**, *5*, 2617–2638.
64. Quan, X.; He, B.; Li, X.; Yin, C.; Liao, Z.; Xing, M. Retrieval of canopy water content using multiple priori information. In Proceedings of the 2014 IEEE International Geoscience and Remote Sensing Symposium (IGARSS), Québec, QC, Canada, 13–18 July 2014; pp 1863–1866.
65. Carlson, T.N.; Gillies, R.R.; Perry, E.M. A method to make use of thermal infrared temperature and NDVI measurements to infer surface soil water content and fractional vegetation cover. *Remote Sens. Rev.* **1994**, *9*, 161–173.
66. Ray, R.L.; Jacobs, J.M.; Cosh, M.H. Landslide susceptibility mapping using downscaled AMSR-E soil moisture: A case study from Cleveland Corral, California, US. *Remote Sens. Environ.* **2010**, *114*, 2624–2636.
67. Chauhan, N.; Miller, S.; Ardanuy, P. Spaceborne soil moisture estimation at high resolution: A microwave-optical/IR synergistic approach. *Int. J. Remote Sens.* **2003**, *24*, 4599–4622.



68. Piles, M.; Camps, A.; Vall-Llossera, M.; Corbella, I.; Panciera, R.; Rudiger, C.; Kerr, Y.H.; Walker, J. Downscaling SMOS-derived soil moisture using MODIS visible/infrared data. *IEEE Trans. Geosci. Remote Sens.* **2011**, *49*, 3156–3166.
69. Zhang, Y.; Guindon, B.; Cihlar, J. An image transform to characterize and compensate for spatial variations in thin cloud contamination of Landsat images. *Remote Sens. Environ.* **2002**, *82*, 173–187.
70. Zhang, A.; Jia, G. Monitoring meteorological drought in semiarid regions using multi-sensor microwave remote sensing data. *Remote Sens. Environ.* **2013**, *134*, 12–23.
71. Earth Resources Observation and Science Center. Available online: <http://glovis.usgs.gov/> (accessed on 12 September 2014).
72. Li, X.; He, B.; Quan, X.; Liao, Z.; Bai, X. Use of the standardized precipitation evapotranspiration index (SPEI) to characterize the drying trend in southwest China from 1982–2012. *Remote Sens.* **2015**, *7*, 10917–10937.

© 2015 by the authors; licensee MDPI, Basel, Switzerland. This article is an open access article distributed under the terms and conditions of the Creative Commons Attribution license (<http://creativecommons.org/licenses/by/4.0/>).